SHINY CONTACT/
DISTRIBUTED FEEDBACK SEMICONDUCTOR LASERS

By

HORNG-JYE LUO

A DISSERTATION PRESENTED TO THE GRADUATE SCHOOL
OF THE UNIVERSITY OF FLORIDA IN PARTIAL FULFILLMENT
OF THE REQUIREMENTS FOR THE DEGREE OF
DOCTOR OF PHILOSOPHY

UNIVERSITY OF FLORIDA

1993

ACKNOWLEDGMENTS

First of all I wish to express my sincere gratitude to the chairman of my supervisory committee, Dr. P. Zory, for his expert guidance of my research. I am also grateful to Dr. U. Kurzweg, Dr. S. Li, Dr. T. Nishida and Dr. R. Srivastava for serving on my supervisory committee and giving me helpful suggestions.

Thanks are due all my colleagues in the Photonics Research Laboratory for their inspiration and encouragement.

I am indebted to my parents, brothers and sisters for their constant moral support; in particular to my mother for taking good care of my lovely daughter Shertin since last year.

The financial support from the Florida High Technology and Industrial Council and the epitaxial laser materials from Lasertron are gratefully acknowledged.

Last but not least, I want to express the greatest appreciation to my wife Teresa for her love and patience throughout the years in Gainesville. I could not have accomplished this without her understanding.

TABLE OF CONTENTS

Abstract of Dissertation Presented to the Graduate School
of the University of Florida in Partial Fulfillment of the
Requirements for the Degree of Doctor of Philosophy

SHINY CONTACT/DISTRIBUTED FEEDBACK SEMICONDUCTOR LASERS

By

HORNG-JYE LUO

August 1993

Chairman: Peter Zory
Major Department: Electrical Engineering

Shiny contact diode lasers have been demonstrated for
the first time in the 1.3μm InGaAsP/InP material system.
Power levels greater than one watt pulsed have been achieved
at room temperature. Using measured parameters, improvements
in continuous wave performance levels relative to
conventional devices are predicted. The advantages of
combining the shiny contact with the distributed feedback
(DFB) laser structure are described. Ray optics and Floquet-
Bloch formalisms are developed to model the lasing properties
of these shiny contact DFB lasers as well as conventional DFB
lasers. It is shown that the ray optics and Floquet-Bloch
formalisms are superior to the standard overlap integral and
transfer matrix techniques in strong coupling configurations.
The ray optics formalism is extended to deep groove gratings,
of potential use in fabricating low threshold current,
grating surface emitting laser arrays.

CHAPTER I
INTRODUCTION

Semiconductor diode lasers, due to their small size, are extremely "hot" devices. For example, the intensity at the output facet of a 1mW diode laser is comparable to that at the surface of the sun [Zor92]. Therefore, heat dissipation is a critical issue in the design of continuous wave (CW) diode lasers for high power or high temperature applications such as analog communications, optical recording, tunable spectroscopic systems and pump sources for solid state lasers.

The maximum CW output power of a diode laser is limited by two factors: catastrophic optical damage [Hen79] and thermal roll-over [Tod86]. The performance of long wavelength diode lasers such as InGaAsP/InP is usually more sensitive to the temperature variation than that of short wavelength lasers such as AlGaAs/GaAs. When these long wavelength lasers are operated at high power levels, the internal heating raises the temperature of the active layer, causing the threshold current to increase and efficiency to decrease, which further elevates the temperature. Hence the maximum CW output power is usually limited by thermal roll-over. Since the temperature sensitivity for double-heterostructure (DH) lasers is basically a material parameter

and cannot be changed for a given material system, one possible solution to increase the output limit of thermal roll-over is to lower the thermal impedance between the heat source (active layer) and the heat sink (copper block). This can be done using the shiny contact laser structure [Zor75] in which the thermal impedance is minimized by the use of a thin cladding layer. In this work, the first operation of such devices in the 1.3μm InGaAsP/InP material system is demonstrated and power levels greater than 1W pulsed achieved at room temperature. This is among the highest power levels ever reported for single element InGaAsP/InP DH lasers and is comparable to those produced by high power separate confinement heterostructure (SCH) single quantum well (SQW) InGaAsP lasers operating at 1.3μm [Zor93].

By combining the shiny contact with the distributed feedback (DFB) laser structure, more advantages can be expected such as higher device reliability, better single frequency yield and lower fabrication cost compared with conventional type DFB lasers [Luo90]. The shiny contact DFB laser is different from conventional DFB lasers in that the diffraction grating is a corrugated metal/semiconductor interface as opposed to a corrugated semiconductor/semiconductor interface. In conventional DFB lasers, the dielectric grating is only about 0.1μm from the active layer, so the defect states on the corrugated surface may propagate into the active layer during the high temperature epitaxial regrowth after grating fabrication. In

the shiny contact DFB laser configuration, the diffraction grating is placed about an optical wavelength (0.3~0.5μm) from the active layer and the ohmic contact is made directly on top of the grating. Thus the fabrication cost is reduced and the reliability issue is avoided since no epitaxial regrowth is required.

In modeling laser action in DFB devices, one normally utilizes coupled mode theory [Kog72]. In this theory, the key laser parameter is the backward coupling coefficient κ since its magnitude determines such parameters as frequency selectivity and threshold mode gain. The standard technique to determine κ in a DFB laser is to evaluate the coupled mode integral which describes the overlap of the unperturbed mode with the grating perturbation [Str75]. It has been shown that this technique shows an inherent problem as to how to choose the unperturbed waveguide geometry when the perturbation is strong [Str77] [Cor88]. For example, in semiconductor/metal or semiconductor/air gratings where the refractive index difference is large, the standard approach gives results strongly dependent on the choice of the unperturbed waveguide [Sha89]. Another widely used method, the effective index transfer matrix method [Han92], shows difficulties in considering transverse modes and ambiguities in the transformation for highly asymmetrical corrugated waveguides.

As a result, ray optics and Floquet-Bloch formalisms are developed to model the lasing properties of the shiny contact

DFB structure where standard techniques fail. The ray optics formalism is also used to derive closed form expressions for the coupling coefficient in conventional type DFB structures with dielectric gratings [Luo93]. In such weak coupling DFB configurations, the κ values obtained from the ray optics expression, transfer matrix and overlap integral approaches show excellent agreement. The ray optics formalism is superior to standard techniques because it provides device designers with closed-form expressions in both strong and weak coupling DFB configurations, and it can be extended to deep groove gratings.

Grating surface emitting (GSE) lasers can be integrated into two dimensional arrays and are widely used in high power applications such as pump sources for solid state lasers. In the conventional design with shallow groove gratings, however, the threshold current is high due to the presence of the radiation loss. Therefore GSE lasers have not been utilized in low power applications such as chip-to-chip communications [Tak92]. Using the extended ray optics formalism, the first low threshold design of GSE lasers is proposed based on deep groove shiny contact gratings. These structures could be competitive with vertical cavity surface emitting lasers (VCSEL) [Jew91].

This dissertation is organized as follows. In the second chapter, the fabrication and operation of $1.3\mu m$ InGaAsP/InP shiny contact DH lasers are discussed, and the experimental data successfully explained by the theory.

Using the parameter values extracted from the measurements, the improvements in high power CW performance levels relative to conventional devices are predicted.

Chapter III discusses the application of the Floquet-Bloch formalism to the shiny contact DFB laser. The general formalism is truncated by including only the minimum number of terms and applied to several special configurations.

In Chapter IV, closed-form expressions for the DFB coupling coefficient are derived using the ray optics formalism in shiny contact and conventional DFB laser configurations. Numerical results using the Floquet-Bloch, ray optics and standard techniques are compared in various DFB structures.

Then the deep groove effects are investigated in Chapter V. The ray optics formalism is extended to design the deep groove shiny contact GSE laser.

Finally, Chapter VI contains conclusions and recommendations for future research.

CHAPTER II
HIGH POWER InGaAsP/InP SHINY CONTACT DIODE LASERS

It is well known that the experimentally observed
threshold current I_{th} for double heterostructure (DH) diode
lasers has the following temperature dependence [Cas78]:

$$I_{th} \propto \exp(T/T_0) \tag{2.1}$$

where T is the temperature of the active layer of the laser
and T_0 the characteristic temperature. Generally speaking,
long wavelength lasers have a low value of T_0. For example,
$T_0 \approx 170K$ for AlGaAs/GaAs DH lasers and $T_0 \approx 55K$ for InGaAsP/InP
DH lasers around room temperature [Agr86]. This indicates
that the performance of InGaAsP lasers is much more sensitive
to temperature than that of AlGaAs lasers. To explain the
stronger temperature dependence for InGaAsP lasers, various
mechanisms have been proposed and investigated, such as Auger
recombination [Sug82], leakage current [Yan81], free carrier
absorption [Asa81] and intervalence band absorption [Asa83].
No matter which mechanism is dominant and responsible for the
lower value of T_0, this phenomenon causes thermal roll-over
to limit the highest CW power achievable for InGaAsP/InP
diode lasers, in contrast to AlGaAs/GaAs lasers where
catastrophic optical damage is usually the limiting factor.
This is due to the elevated temperature in the active layer

under high power CW operation since not all of the input electrical power is emitted as light but a large fraction of it is converted into heat. When the temperature of the active layer is increased, the threshold current increases and efficiency decreases, which further raises the temperature. Hence the thermal roll-over sets a limit for InGaAsP/InP lasers in high power or high temperature applications.

Since the characteristic temperature T_0 for DH lasers is basically a material parameter and can not be changed for a given material system, one possible way to improve the thermal roll-over limit is to lower the thermal impedance between the heat source (active layer) and the heat sink. In conventional diode lasers, the thickness of the cladding layer is usually 1.5μm and is far more than enough [Beh90]. In this chapter, we propose and demonstrate a shiny contact laser structure where the thermal impedance is minimized with the use of a thin cladding layer. Reduction of the thickness of the top clad offers several advantages. First of all, the heat generated in the active layer is more efficiently removed because the thermal impedance is minimized. Consequently, devices of this type can produce higher power, operate at higher temperature, and have better reliability and durability. Secondly, a thin cladding layer requires less epitaxial growth time and source material. This is especially attractive for the molecular beam epitaxy (MBE). Other advantages become obvious when the shiny contact is

combined with the distributed feedback (DFB) laser structure, and are presented in the next chapter.

The main problem of such laser structures is the fabrication of the shiny contact, which must have both low electrical resistance and low optical loss. We show that this problem can be solved and both theoretical and experimental results of 1.3µm InGaAsP/InP shiny contact diode lasers are given. Power levels greater than one watt pulsed have been achieved at room temperature. To the best of our knowledge, this is the first demonstration of such devices in 1.3µm InGaAsP/InP. The power levels we have achieved are comparable to those obtained from quantum well InGaAsP/InP lasers [Zor93]. Section 2.1 discusses the theoretical design of the shiny contact laser structure, followed by discussions of the fabrication procedures and experimental results. Finally the potential impact of such laser structures is predicted.

2.1 Theoretical Analysis of Shiny Contact Lasers

Figure 2-1 shows the DH type InGaAsP/InP laser structure and relevant parameters used throughout the theoretical analysis. The complex refractive index of gold is obtained from [Pal85], and the extinction index of the ternary InGaAs is derived from an estimated absorption of 6700/cm at lasing wavelength $\lambda=1.3$µm. The thickness of the contact layer is the minimum value required for a good ohmic contact as

determined by the depletion width of the metal-semiconductor junction. Gold is the natural candidate for the contact metal due to its superior electrical and optical properties. The p-clad thickness t is the main variable whose value is to be optimized.

To investigate the effects on the laser performance when t is reduced, the two key factors are the optical mode confinement factor Γ and the optical mode loss α_m due to the metalization (introduced by the contact layer and the contact metal). These two factors directly affect the threshold current and efficiency of a laser. In general one wants to minimize the loss but maximize the confinement.

The optical mode loss due to the metalization can be calculated by solving the transcendental eigenvalue equation for the five layer waveguide structure [Tam90]:

$$\exp(2p_2t)\frac{(p_0p_2+p_1^2)\sinh(p_1h) + p_1(p_2+p_0)\cosh(p_1h)}{(p_0p_2-p_1^2)\sinh(p_1h) + p_1(p_2-p_0)\cosh(p_1h)}$$

$$= \frac{(p_2p_4-p_3^2)\sinh(p_3d) + p_3(p_2-p_4)\cosh(p_3d)}{(p_2p_4+p_3^2)\sinh(p_3d) + p_3(p_2+p_4)\cosh(p_3d)} \tag{2.2}$$

where

$$p_i = \sqrt{\beta_o^2 - n_i^2k^2} \qquad i=0,1,2,3,4$$

$$k = 2\pi/\lambda \qquad \lambda: \text{ wavelength in vacuum}$$

$$\beta_o = n_{eff}\,k \qquad n_{eff}: \text{ effective waveguide index}$$

The loss due to the free carrier absorption in the metal and the band-to-band absorption in the contact layer are included in the complex refractive indices, and therefore the optical

mode loss α_m of the waveguide is directly related to the imaginary part of the propagation constant β_0,

$$\alpha_m = 2\,\mathrm{Im}(\beta_0) \tag{2.3}$$

In Figure 2-2 the calculated results for α_m are plotted as a function of the p-clad thickness t. It is observed that α_m increases monotonically as t decreases. However, since the internal optical loss for 1.3μm InGaAsP DH lasers is typically around 30cm^{-1}, the extra loss introduced by the metalization can be neglected for t≥0.4μm.

The optical mode confinement factor Γ is defined as the proportion of the optical mode overlapping with the active layer where optical gain is present:

$$\Gamma = \frac{\int_0^d |E(x)|^2\,dx}{\int_{-\infty}^{\infty} |E(x)|^2\,dx} \tag{2.4}$$

where E(x) is the electric field distribution for the transverse mode of interest. One can solve E(x) then numerically integrate eq.(2.4) to obtain Γ. Alternatively, one can put a small material gain Δg in the active layer and solve for the complex propagation constant of the waveguide, then Γ is the relative increase in the mode gain ΔG per unit Δg. The latter technique is utilized to obtain the results shown in Figure 2-3. It is seen that as t is reduced, Γ increases slowly in the beginning then goes down suddenly. There is a maximum value for Γ occurring at t≈0.2μm. This phenomenon can be attributed to the competition between the

effects of the shiny contact and the twin guide formed by the active and contact layers. When t is reduced, the metal tends to push the optical mode downward while the formation of the twin guide tends to trap the optical power. The latter effect dominates for $0.5\mu m > t > 0.2\mu m$. As t is smaller than $0.2\mu m$, however, the effect of the shiny metal becomes dominant and the optical mode is pushed away so Γ drops sharply.

The threshold mode gain G_{th} and the threshold material gain g_{th} for a laser are

$$\Gamma g_{th} = G_{th} = \alpha_i + \alpha_m + \frac{1}{L} \ln(\frac{1}{R})$$

$$= \alpha_t + \frac{1}{L} \ln(\frac{1}{R}) \qquad (2.5)$$

where $\alpha_i = 30 cm^{-1}$ is the internal optical loss due to free carrier absorption, α_t the total optical mode loss, $L = 250\mu m$ the cavity length and $R = 0.32$ the facet reflectivity. The carrier density at threshold N_{th} can be empirically approximated as the following function of g_{th} [Dut82]:

$$N_{th} \cong 1.103 \times 10^{18} + 6.445 \times 10^{15} \cdot g_{th} - 3.856 \times 10^{13} \cdot g_{th}^2$$

$$+ 1.768 \times 10^{11} \cdot g_{th}^3 - 4.156 \times 10^{8} \cdot g_{th}^4 + 3.993 \times 10^{5} \cdot g_{th}^5 \qquad (2.6)$$

where N_{th} is in $1/cm^3$ and g_{th} in $1/cm$. The radiative and nonradiative current density can be written as [Dut82]

$$J_r = \frac{d}{\beta} \left(g_{th} + \beta j_{tr} \right) \qquad (2.7)$$

$$J_{nr} = e \, d \, C \, N_{th}^3 \qquad (2.8)$$

where $\beta \cong 0.0783 cm \cdot \mu m/A$ and $j_{tr} \cong 3000 A/cm^2 \cdot \mu m$ are calculated gain parameters and $C \cong 3.0 \times 10^{-29} cm^6/s$ the Auger coefficient for

InGaAsP [Agr86]. The threshold current density J_{th} and the differential quantum efficiency η_d are then

$$J_{th} = \eta_i \ (J_r + J_{nr}) \equiv \eta_i \ \eta_r \ J_r \equiv \eta_{sp} \ J_r \qquad (2.9)$$

$$\eta_d = \eta_i \ \frac{\frac{1}{L} \ln(\frac{1}{R})}{G_{th}} \qquad (2.10)$$

where η_i is the injection efficiency defined as the fraction of carriers injected into and recombined in the active layer, η_r the radiative efficiency (or internal quantum efficiency) defined as the fraction of injected carriers recombined as photons, and η_{sp} the spontaneous efficiency - the product of η_i and η_r. These parameters can be extracted from the experimental data (see Section 2.3) and we assume $\eta_i=1$ in this section.

The calculated threshold current density and differential quantum efficiency are presented in Figures 2-4 and 2-5 respectively. It is interesting to note from Figure 2-4 that as t decreases, J_{th} actually goes down a little bit before it rises up sharply. This is due to the fact that the increase in the optical mode loss is more than offset by the improvement in the confinement factor as one reduces the p-clad thickness. Since this effect is very subtle, one can generally assume that J_{th} is constant at t≥0.4μm. The differential quantum efficiency decreases monotonically as t decreases but does not change much until t<0.5μm. The reduction of η_d simply comes from the increase in α_t.

From the above theoretical analysis, we see that the p-clad thickness in conventional diode laser is much larger than needed. In principle one can improve the high power CW performance of InGaAsP DH lasers by using a thin p-clad of about 0.5μm without degrading such properties as threshold current density and differential quantum efficiency. In the next section the fabrication procedures of such shiny contact lasers in InGaAsP/InP are discussed.

2.2 Fabrication of Shiny Contact Lasers

Wide-stripe gain-guided InGaAsP/InP shiny contact lasers were fabricated from Wafer QA21125 grown by Lasertron using liquid phase epitaxy (LPE). A schematic diagram for the DH laser structure is shown in Figure 2-6 where all relevant parameter values are given. The processing techniques are described as follows.

The SiO_2 coated wafer was originally about 400μm thick and was lapped down to about 100μm in thickness using 9μm Al_2O_3 powder. During the lapping process, the wafer were surrounded by 3 GaAs dummy stacks, each of which contained 2 GaAs pieces adhered together by photoresist. Since InP based materials are softer than GaAs, a lower lapping speed ~10rpm was used.

The wafer was then cleaned in heated TCA, acetone, methanol and IPA, rinsed in DI water and blown dry using a nitrogen gun. After dehydrating at 110°C for 30 minutes, the

wafer was placed on a cover glass which had been spun coated with photoresist 1350J at 2000rpm for 15 seconds. The glass-wafer was baked at 90°C for 10 minutes so that the wafer would not drop during processing. Then photoresist 1350J was spun coated on SiO_2 of the wafer at 5000rpm for 30 seconds, and a soft bake was performed at 90°C for 20 minutes. After an exposure of 10 seconds with the mask on the front (SiO_2 side) and 1 minute without the mask on the back (through the cover glass), the glass-wafer was developed at 1:7.5 diluted developer 606 for 12 seconds and the wafer was separated from the glass. The wafer was rinsed, blown dry and hard baked at 110°C for 20 minutes before chemically etched in BOE(6:1) for 2 minutes and 45 seconds to open a 100μm window in the SiO_2 layer.

Immediately following another rinsing and blowing, the epitaxial side was e-beam evaporated with 1500Å gold at 3Å/sec with liquid nitrogen in the diffusion pump. A lift-off was then done in hot acetone so that only the gold on top of the window (in direct contact with the contact layer) was left. After a regular cleaning procedure, the whole oxide side was coated with 1000Å nickel and 500Å gold. Finally the substrate side was coated with 2000Å gold.

The wafer was cleaved into bars of cavity length ranging from 125μm to 500μm using our standard cleaving techniques: scribe, roll and break. The cleaved bars were probe tested before they were diced into laser chips. Then some of the chips were attached to copper blocks using silver epoxy at

around 90°C. The test results are given in the next section along with comparison with the theory.

2.3 Experimental Results

The probe test on the cleaved bars reveals that the threshold current is very uniform across the wafer. The measured P-I characteristic (power vs. current) for these shiny contact lasers at 300K is plotted in Figure 2-7 for different cavity lengths under 0.5μs pulse at 1kHz. The lasers with L=125μm produce 1.1W power at current of 2A, and the 500μm ones produce 0.5W at 2A. These power levels are among the highest for InGaAsP/InP DH lasers, and are close to those obtained from state-of-the-art separate confinement heterostructure (SCH) single quantum well (SQW) lasers [Zor93]. Figure 2-8 shows the inverse of the slope efficiency vs. cavity length. The slope efficiency η_s is defined as the relative increase in the optical power with the input current in the P-I curve beyond threshold,

$$\eta_s = \frac{\Delta P}{\Delta I} = V_c \, \eta_d = V_c \, \eta_i \frac{\ln(1/R)}{\alpha_t L + \ln(1/R)} \qquad (2.11)$$

where V_c is the characteristic voltage (the voltage corresponding to the bandgap). The measured η_s in Figure 2-8 is curve fitted as

$$\eta_s^{-1} = 1.278 + 0.00245L \qquad (2.12)$$

where η_s is in W/A and L in μm. Comparing eqs. (2.12) with (2.11), one gets $\alpha_t = 22\text{cm}^{-1}$ and $\eta_i = 82\%$, very reasonable values

in good agreement with the theoretical assumption in the previous section. Such a low value for α_t indicates that the shiny contact introduces negligible optical loss, consistent with the theoretical calculations in Section 2.1. The threshold current is plotted in Figure 2-9 as a function of cavity length. It is seen that the experimental data is fitted as the following expression

$$I_{th} = 153.5 + 1.184L \qquad (2.13)$$

where I_{th} is in mA and L in μm. Compare this equation with the theory,

$$I_{th} = Lwd\left[\frac{\alpha_t}{\eta_{sp}\beta\Gamma} + \frac{j_{tr}}{\eta_{sp}}\right] + \frac{wd\ln(1/R)}{\eta_{sp}\beta\Gamma} \qquad (2.14)$$

one obtains $\eta_{sp}\beta = 0.0275$cm$\cdot\mu$m/A and $j_{tr}/\eta_{sp} = 4446$A/cm$^2\cdot\mu$m. Assume the calculated value for j_{tr} is 3000A/cm$^2\cdot\mu$m, then $\eta_{sp} = 67\%$ and hence $\eta_r = 82\%$. The Auger coefficient and the gain slope should be C$=1.6\times10^{-29}$cm^6/s and $\beta = 0.0334$cm$\cdot\mu$m/A. One can see that both C and β are overestimated in the theory by about 88% and 135% respectively. Both the theoretical and experimental results for C and β are in the same order of magnitude and are reasonably close, considering the uncertainties in the energy band structure for InGaAsP [Kat92].

The P-I curve for the L$=250\mu$m laser at different temperatures is plotted in Figure 2-10, and the temperature dependence of the threshold current and slope efficiency given in Figures 2-11 and 2-12 respectively. It is clear

that the threshold current and slope efficiency can be approximated as

$$I_{th} = 300 \exp(T/59) \qquad\qquad (2.15)$$

$$\eta_s = 0.641 - 0.00276T \qquad\qquad (2.16)$$

where I_{th}, η_s and T are in mA, W/A and °C respectively. The measured characteristic temperature $T_0 = 59$°C and the temperature dependence of η_s agree excellently with previous reports [Agr86].

In the next section we discuss the expected improvements in the CW performance for such shiny contact lasers relative to conventional DH lasers using parameter values extracted from the measurements presented in this section.

2.4 Further Discussion

In Section 2.3 it has been shown that the pulsed performance of the 1.3μm InGaAsP/InP shiny contact laser is consistent with the theoretical predictions. In this section, the CW performance for such lasers is investigated at room temperature, in which case the thermal impedance is a key parameter.

According to the analysis presented in Section 2.1, the optimal p-clad thickness for a 1.3μm InGaAsP/InP shiny contact laser structure should be t=0.5μm. In applications where single mode operation is preferred, the cavity length and the window width should not be too large. Therefore in

this section a shiny contact structure with the following dimension parameters is assumed: $t=0.5\mu m$, $L=250\mu m$ and $w=4\mu m$.

First of all, the output power vs. current for a diode laser can be expressed as

$$P_o = \eta_s(I-I_{th}) \tag{2.17}$$

where the threshold current I_{th} and the slope efficiency η_s are assumed to have the following forms, according to our measurements,

$$I_{th} = 0.025 \exp[(T_a-T_s)/59] \quad \text{(in A)} \tag{2.18}$$

$$\eta_s = 0.48 \left[\frac{232-T_a}{232-T_s}\right] \quad \text{(in W/A)} \tag{2.19}$$

where T_a and T_s are the temperatures in °C of the active layer and the heat sink respectively ($T_s=27°C$). A lower injection efficiency (70%) has been used for such a narrow stripe structure to account for the lateral current flow. The I-V (current-voltage) relation of a diode laser is

$$V = V_c + I\,r_d \tag{2.20}$$

where $V_c=1V$ and $r_d=10\Omega$ are assumed. Note that not all of the input electrical power is emitted as light but a large fraction of it is converted into heat; hence, one may write

$$\dot{Q} = V\,I - P_o = (T_a-T_s)/R_{th} \tag{2.21}$$

where $\dot{Q}$ is the thermal power (heat flux) and R_{th} the thermal impedance. If R_{th} is known, eqs. (2.17)-(2.21) can be solved self consistently to obtain the actual temperature in the active layer T_a at a given current, from which the output power P_o is then calculated.

The thermal impedance can be estimated by assuming that most of the heat is generated in the center of the active layer and flows through the epitaxial layers to the heat sink one dimensionally [Kre77]. In this case, the thermal impedance of each layer can be written as ρ_{th} d/A where ρ_{th} is the thermal resistivity, d the length along the heat flow and A the area of the cross section. The following values are used in the calculations [Kat92]: ρ_{th}=1.47cm·K/W for InP, ρ_{th}=20.9cm·K/W for $In_{.53}Ga_{.47}As$ and ρ_{th}=22.5cm·K/W for $In_{.73}Ga_{.27}As_{.6}P_{.4}$. The copper block accounts for about 18K/W approximately [Kre77]. The experimentally measured data for R_{th}, however, generally agrees with those obtained using a two dimensional analysis [Yan81], which shows that R_{th} should be about one half of that calculated one dimensionally for a narrow stripe laser. Therefore we estimate R_{th} to be 40K/W for the shiny contact laser (h=300Å and t=0.5μm) and 100K/W for the conventional laser (h=0.5μm and t=1.5μm).

The predicted CW power vs. current is plotted in Figure 2-13. Obviously, both the linearity and highest output power are shown to be greatly improved using the shiny contact laser structure. This figure confirms that in conventional InGaAsP/InP DH laser structures, the high power or high temperature performance is limited by the heating effect due to the large thermal impedance. For example, at I=100mA, the temperature in the active layer is 43°C for the conventional laser while it is 33°C for the shiny contact laser-- improvement of 10°C can be obtained. At higher current

levels, the improvement is even bigger: T_a is 81°C vs. 47°C at 200mA and 143°C vs. 70°C at 300mA.

In conclusion, we have demonstrated the first operation of shiny contact lasers in the 1.3μm InGaAsP/InP system, and achieved power levels greater than 1W pulsed at current of 2A at room temperature – comparable to those obtained from state-of-the-art single quantum well lasers. The experimental data has been successfully modeled using the theory, and important parameters extracted from the measurements. The improvements in the CW performance for such shiny contact lasers relative to conventional devices are predicted using these measured parameters.

metalization: gold	$n_0 = 0.41 - i8.3$	
contact: $In_{.53}Ga_{.47}As$	$n_1 = 3.60 - i0.007$	$h = 300 \text{Å}$
p-clad: InP	$n_2 = 3.20$	t
active: $In_{.73}Ga_{.27}As_{.6}P_{.4}$	$n_3 = 3.52$	$d = 0.2 \mu m$
n-clad: InP	$n_4 = 3.20$	

$$\lambda = 1.3 \mu m$$

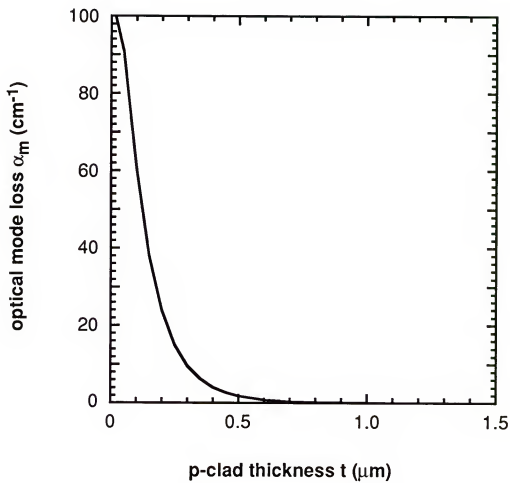Figure 2-1: The InGaAsP/InP DH laser structure
used in the theoretical analysis

Figure 2-2: The extra optical mode loss
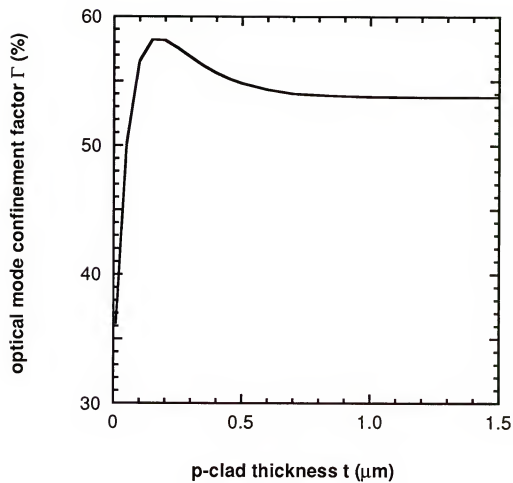for the structure shown in Figure 2-1

Figure 2-3: The optical mode confinement factor
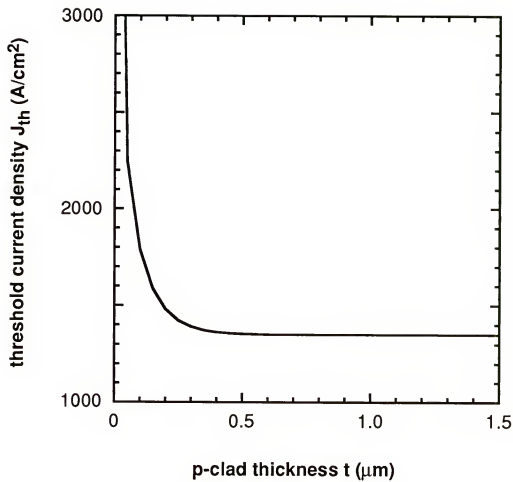for the structure shown in Figure 2-1

Figure 2-4: The threshold current density
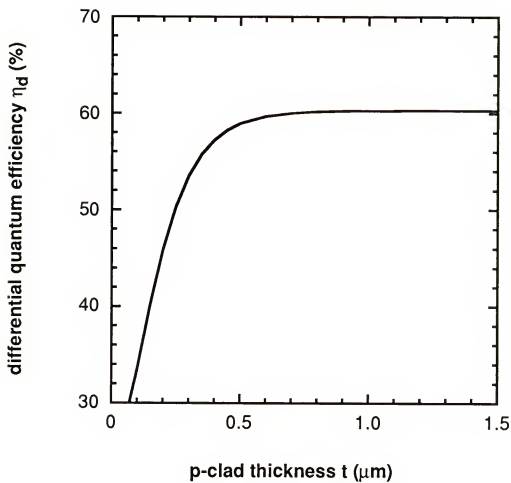for the structure shown in Figure 2-1

Figure 2-5: The differential quantum efficiency
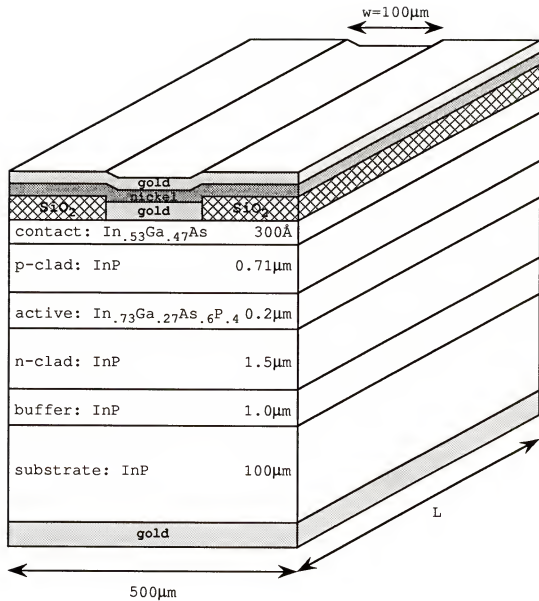for the structure shown in Figure 2-1

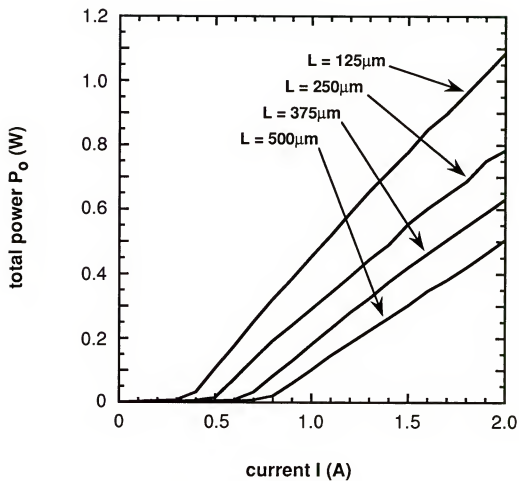Figure 2-6: A schematic view of the shiny contact laser

Figure 2-7: The measured total power vs. current for the
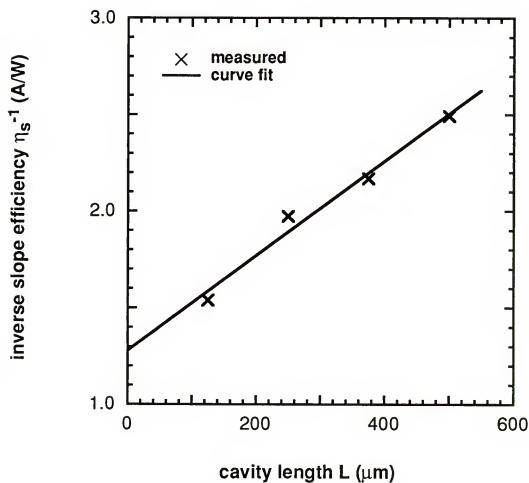InGaAsP shiny contact lasers fabricated at UF

Figure 2-8: The inverse slope efficiency vs. cavity length
for the InGaAsP shiny contact lasers fabricated at UF
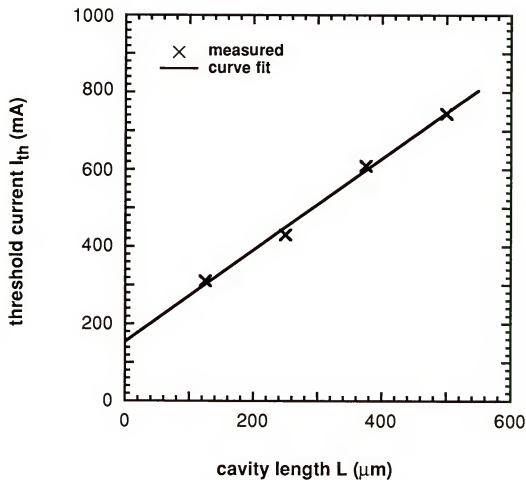
Figure 2-9: The threshold current vs. cavity length for the InGaAsP shiny contact lasers fabricated at UF

Figure 2-10: The measured total power vs. current
for the L=250μm laser at different temperatures

Figure 2-11: The threshold current as a function of temperature for the L=250μm shiny contact laser

Figure 2-12: The slope efficiency as a function of temperature
for the L=250μm shiny contact laser

Figure 2-13: The calculated CW power vs. current plot
for the optimized InGaAsP shiny contact laser

CHAPTER III
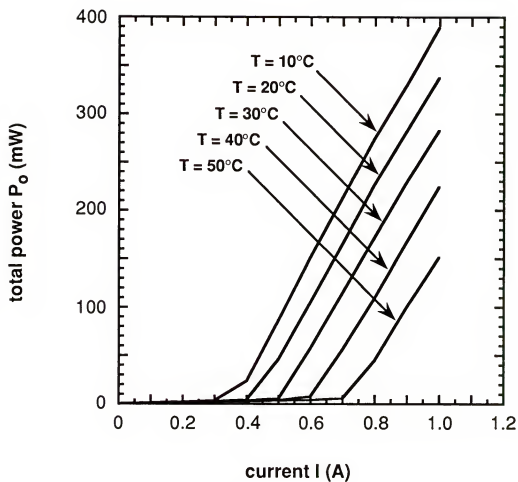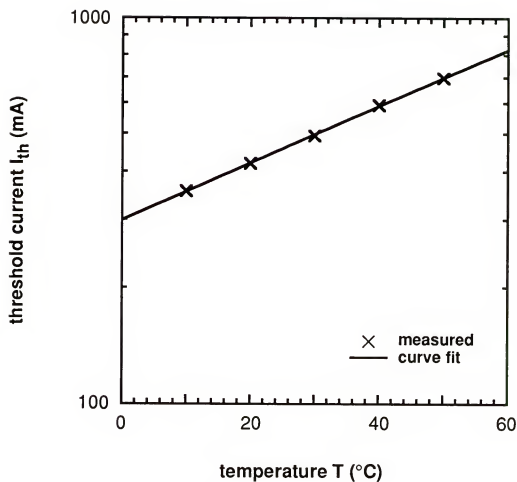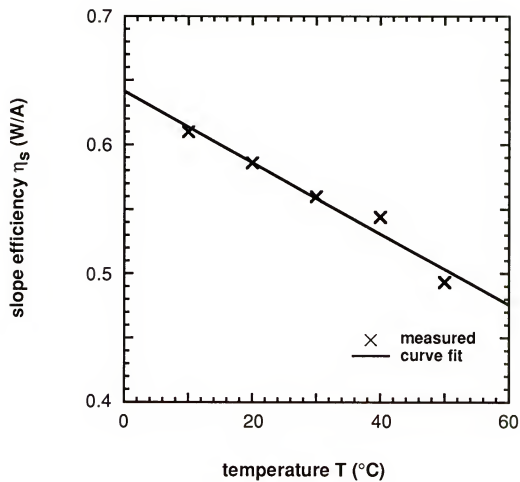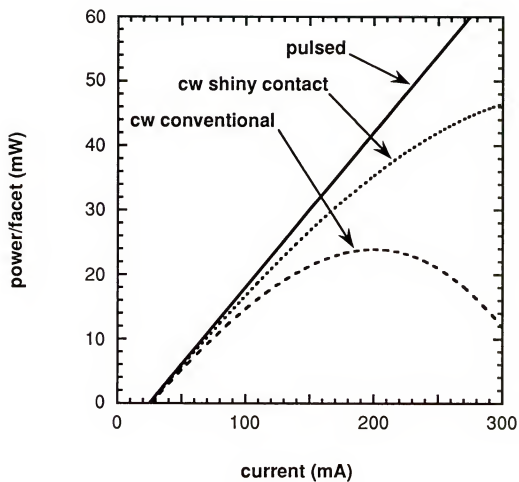FLOQUET-BLOCH ANALYSIS OF THE SHINY CONTACT
DISTRIBUTED FEEDBACK DIODE LASER

In the previous chapter, the operation of 1.3μm InGaAsP/InP shiny contact lasers has been demonstrated for the first time, and several advantages of such devices described. In this chapter, we discuss a shiny contact distributed feedback (DFB) laser structure in which the diffraction grating is a corrugated metal/semiconductor interface as shown in Figure 3-1. Heterostructure diode lasers with such integrated, metalized diffraction gratings were first demonstrated about eighteen years ago [Zor75, Wal77]. The two main reasons for using metalized gratings instead of dielectric gratings are thermal impedance minimization and elimination of epitaxial regrowth after grating fabrication. The former has been explained in Chapter II, and the latter could not only reduce the fabrication cost but also improve the reliability. In conventional DFB lasers, the diffraction grating is only about 0.1μm from the active layer and one has to perform a high temperature epitaxial regrowth process after grating fabrication. The high temperature regrowth on a corrugated interface can possibly diffuse the surface defects into the active layer and hence introduces a reliability problem. In

34

the shiny contact DFB laser configuration, the diffraction grating is placed about an optical wavelength (dimension t≈0.3~0.5µm in Figure 3-1) from the active layer and the ohmic contact is made directly on top of the grating, thus the fabrication cost is reduced and the reliability issue is avoided since no epitaxial regrowth is required.

Other advantages of using such metalized gratings include better single frequency yield for edge emitting DFB lasers [Sha89] and higher CW power for grating surface emitting (GSE) lasers [Mac87]. The former is due to the combined index/loss DFB coupling mechanism built in the metalized grating, which is absent in conventional type DFB lasers using dielectric gratings. The latter is because there is only one radiation beam reflecting from the metalized grating, in contrast with two radiation beams (one upward and one downward) from conventional GSE lasers with dielectric gratings, and one of the two beams is not utilized.

The main problem with metalized gratings is that the corrugated metal/semiconductor interface must have low electrical resistance and low optical mode loss--shiny contact grating. Our experiment shows that this problem can be solved [Luo92] and recent reports indicate that high performance, reliable devices have been fabricated [Sha88, Mot89, Ras91].

In modeling laser action in DFB devices, one normally utilizes coupled mode theory [Kog72] or transfer matrix

approach [Han92]. These standard techniques do not work well in the shiny contact DFB structure due to the large index difference at such metalized gratings (see Chapter IV). As a result, a Floquet-Bloch formalism [Nol90] is developed in this chapter to analyze the wave propagation in the shiny contact DFB laser. The full Floquet-Bloch expansion is truncated by including only the minimum number of terms and applied to several practical configurations. Numerical results are presented in the next chapter for comparison with those obtained using the ray optics and standard approaches.

3.1 Full Floquet-Bloch Formalism

The configuration used in the analysis is that of a perfect metal clad sinusoidally corrugated waveguide for TE modes, i.e., the electric field is y-oriented in Figure 3-1. Assume the electric field mode in each layer is expanded using the following plane wave series based on Floquet-Bloch theorem:

$$E_d(x,z) = \sum_{m=-\infty}^{\infty} A_m \exp[-q_m(x-t-d)]\exp(-i\beta_m z)$$

$$E_a(x,z) = \sum_{m=-\infty}^{\infty} \left\{ B_m \cos[\sigma_m(x-t)] + C_m \sin[\sigma_m(x-t)] \right\} \exp(-i\beta_m z)$$

$$E_b(x,z) = \sum_{m=-\infty}^{\infty} \left\{ D_m \exp(p_m x) + E_m \exp(-p_m x) \right\} \exp(-i\beta_m z)$$

$$E_c(x,z) = 0 \text{ in the perfect metal} \tag{3.1}$$

where

$$\beta_m = \beta_0 + mK = \beta_0 + m(2\pi/\Lambda)$$

$$\sigma_m = \sqrt{n_a^2 k^2 - \beta_m^2}$$

$$p_m = \sqrt{\beta_m^2 - n_b^2 k^2}$$

$$q_m = \sqrt{\beta_m^2 - n_d^2 k^2}$$

$$k = 2\pi/\lambda \qquad \lambda: \text{ wavelength in vacuum}$$

Rayleigh was the first to use a similar plane wave series in analyzing classical diffraction problems and he assumed that such a plane wave series can uniformly converge to the unique solution when the number of terms included goes to infinity, and this assumption is referred as Rayleigh assumption [Pet80]. Despite the fact that Rayleigh assumption is not always true for an arbitrary grating shape, the results obtained using this expansion are generally fast and accurate for sinusoidal groove gratings [Pet80]. Consequently this method is adopted to investigate the wave propagation in the shiny contact DFB structure.

At x=t, the electric field and its derivative should be continuous, and this leads to

$$\sum_{m=-\infty}^{\infty} B_m \exp(-i\beta_m z) = \sum_{m=-\infty}^{\infty} \left\{ D_m \exp(p_m t) + E_m \exp(-p_m t) \right\} \exp(-i\beta_m z)$$

$$\implies B_m = D_m \exp(p_m t) + E_m \exp(-p_m t) \quad \forall m \qquad (3.2)$$

$$\sum_{m=-\infty}^{\infty} \sigma_m C_m \exp(-i\beta_m z) = \sum_{m=-\infty}^{\infty} p_m \left\{ D_m \exp(p_m t) - E_m \exp(-p_m t) \right\} \exp(-i\beta_m z)$$

$$\implies \sigma_m C_m = p_m \left\{ D_m \exp(p_m t) - E_m \exp(-p_m t) \right\} \quad \forall m \qquad (3.3)$$

Similarly at x=t+d,

$$\sum_{m=-\infty}^{\infty} A_m \exp(-i\beta_m z) = \sum_{m=-\infty}^{\infty} \{ B_m \cos(\sigma_m d) + C_m \sin(\sigma_m d) \} \exp(-i\beta_m z)$$

$$\implies \quad A_m = B_m \cos(\sigma_m d) + C_m \sin(\sigma_m d) \quad \forall m \tag{3.4}$$

$$\sum_{m=-\infty}^{\infty} q_m A_m \exp(-i\beta_m z) = \sum_{m=-\infty}^{\infty} \sigma_m \{ B_m \sin(\sigma_m d) - C_m \cos(\sigma_m d) \} \exp(-i\beta_m z)$$

$$\implies \quad q_m A_m = \sigma_m \{ B_m \sin(\sigma_m d) - C_m \cos(\sigma_m d) \} \quad \forall m \tag{3.5}$$

At the grating surface $x=f(z)=a\cos(Kz)$, E_b should vanish since a perfect metal has been assumed,

$$\sum_{m=-\infty}^{\infty} \{ D_m \exp[p_m f(z)] + E_m \exp[-p_m f(z)] \} \exp(-i\beta_m z) = 0 \tag{3.6}$$

Recall the following Fourier series,

$$\exp[\pm p_m a \cos(Kz)] = \sum_{n=-\infty}^{\infty} I_n(\pm p_m a) \exp(inKz)$$

where $I_n(u)$ is the modified (or hyperbolic) Bessel function of the first kind (of order n). The following equations are listed for reference.

$$I_n(-u) = (-1)^n I_n(u)$$

$$I_{-n}(u) = I_n(u)$$

Then eq.(3.6) becomes

$$\sum_{m=-\infty}^{\infty} \exp(-i\beta_m z) \{ D_m \sum_{n=-\infty}^{\infty} I_n(p_m a) \exp(inKz)$$

$$+ E_m \sum_{n=-\infty}^{\infty} (-1)^n I_n(p_m a) \exp(inKz) \} = 0$$

$$\sum_{m=-\infty}^{\infty} \exp(-i\beta_0 z) \left\{ D_m \sum_{n=-\infty}^{\infty} I_n(p_m a) \exp[-i(m-n)Kz] \right.$$

$$\left. + E_m \sum_{n=-\infty}^{\infty} (-1)^n I_n(p_m a) \exp[-i(m-n)Kz] \right\} = 0$$

Since the coefficient of $\exp(-inKz)$ for each n should be zero, one then obtains

$$\sum_{m=-\infty}^{\infty} \left\{ D_m I_{m-n}(p_m a) + E_m(-1)^{m-n} I_{m-n}(p_m a) \right\} = 0 \quad \forall n \qquad (3.7)$$

Equations $(3.2)-(3.5)$ and (3.7) constitute an infinite linear homogeneous system. The number of equations is equal to the number of variables, and therefore a nonzero solution requires that the determinant vanish. Thus a characteristic eigenvalue equation can be obtained and solved for β_0 at each λ--dispersion relation.

In practice only finite terms can be considered in this linear system. Suppose one keeps N orders (there are N values for the order index m), then one gets a 5N×5N matrix! Due to the huge amount of numerical computation involved, it is very difficult to present a general treatment. Consequently, several special cases of practical interest are studied based on a simplified, truncated expansion in the next section. The numerical results obtained using the truncated Floquet-Bloch formalism are given in Chapter IV along with those from the ray optics and other standard techniques for comparison.

3.2 <u>Truncated Floquet-Bloch Formalism</u>

First of all we look at the zeroth order case where only $m=0$ is considered. This case represents an unperturbed, planar four-layer waveguide with a perfect metal clad, i.e., $a=0$. The above linear homogeneous system leads to

$$B_0 - D_0 \exp(p_0 t) - E_0 \exp(-p_0 t) = 0$$

$$\sigma_0 C_0 - p_0 D_0 \exp(p_0 t) + p_0 E_0 \exp(-p_0 t) = 0$$

$$A_0 - B_0 \cos(\sigma_0 d) - C_0 \sin(\sigma_0 d) = 0$$

$$q_0 A_0 - \sigma_0 B_0 \sin(\sigma_0 d) + \sigma_0 C_0 \cos(\sigma_0 d) = 0$$

$$D_0 + E_0 = 0$$

where $I_0(0)=1$ and $I_n(0)=0$ for $n\neq0$ have been used. Requiring a nontrivial solution, this 5×5 system can be manipulated to obtain the following transcendental equation:

$$p_0 \coth(p_0 t) = \sigma_0 \tan[\sigma_0 d - \tan^{-1}(q_0/\sigma_0)] \tag{3.8}$$

Due to the mirror principle, this equation is the same as for the odd mode of a symmetric 5-layer waveguide whose refractive index is $n_d/n_a/n_b/n_a/n_d$ and thickness $\infty/d/2t/d/\infty$. The dispersion curve for such a planar waveguide is shown as the solid line in Figure 3-2.

Next let us consider a first order grating with a shallow groove, i.e., $K=2\beta_0$ and $ka\ll1$. In this case, there are only two traveling terms that carry electromagnetic power: the fundamental forward wave ($m=0$, propagation constant=β_0) and the backward diffracted wave ($m=-1$, propagation constant=$-\beta_0$). All higher order waves are

evanescent along x and fast oscillating along z, and are neglected in the following calculations. This two wave approximation is valid for shallow groove gratings normally utilized in most practical DFB laser configurations. From eqs. (3.2)-(3.5), one has

$$B_0 - D_0 \exp(p_0 t) - E_0 \exp(-p_0 t) = 0$$

$$B_{-1} - D_{-1} \exp(p_{-1} t) - E_{-1} \exp(-p_{-1} t) = 0$$

$$\sigma_0 C_0 - p_0 D_0 \exp(p_0 t) + p_0 E_0 \exp(-p_0 t) = 0$$

$$\sigma_{-1} C_{-1} - p_{-1} D_{-1} \exp(p_{-1} t) + p_{-1} E_{-1} \exp(-p_{-1} t) = 0$$

$$A_0 - B_0 \cos(\sigma_0 d) - C_0 \sin(\sigma_0 d) = 0$$

$$A_{-1} - B_{-1} \cos(\sigma_{-1} d) - C_{-1} \sin(\sigma_{-1} d) = 0$$

$$q_0 A_0 - \sigma_0 B_0 \sin(\sigma_0 d) + \sigma_0 C_0 \cos(\sigma_0 d) = 0$$

$$q_{-1} A_{-1} - \sigma_{-1} B_{-1} \sin(\sigma_{-1} d) + \sigma_{-1} C_{-1} \cos(\sigma_{-1} d) = 0$$

In eq. (3.7), one has to remember that the Bessel function of small argument is fast decaying with increasing order. Hence one needs to pick up the most significant two equations from eq. (3.7). In the present case for first order gratings, one should choose n=0 and n=-1:

$$D_0 I_0(p_0 a) + E_0 I_0(p_0 a) + D_{-1} I_{-1}(p_{-1} a) - E_{-1} I_{-1}(p_{-1} a) = 0$$

$$D_0 I_1(p_0 a) - E_0 I_1(p_0 a) + D_{-1} I_0(p_{-1} a) + E_{-1} I_0(p_{-1} a) = 0$$

After rearrangement, this 10×10 matrix leads to the following eigenvalue equation:

$$\Psi_0 \cdot \Psi_{-1} = \frac{I_0(p_0 a) \cdot I_0(p_{-1} a)}{I_1(p_0 a) \cdot I_1(p_{-1} a)} \tag{3.9}$$

where

$$\Psi_i = \frac{-1}{\tanh\left\{\tanh^{-1}\left\{(\frac{p_i}{\sigma_i})\tan[\sigma_i d + \tan^{-1}(\frac{\sigma_i}{q_i})]\right\} + p_i t\right\}}$$

Since we deal with shallow gratings here, the Bessel functions in eq.(3.9) can be further approximated as polynomials:

$$I_0(u) \cong 1$$
$$\text{for } u \ll 1$$
$$I_1(u) \cong u/2$$

The dispersion curve for such a corrugated waveguide with a first order grating is shown as the thick dashed line in Figure 3.2. It is seen that without the corrugation (perturbation), the ω–β_0 dispersion curve is continuous and smooth. With the perturbation turned on, the interaction between the waveguide mode and the grating introduces a stop band $\Delta\omega$ in the ω–β_0 curve at the Bragg frequency π/Λ. Inside the stop band, the propagation constant β_0 becomes a complex number and the forward wave is attenuated along the corrugated waveguide. This attenuation is due to the continuous feedback under phase matched condition rather than absorption or loss, i.e., the power of the forward wave is continuously reflected into that of the backward wave. The stop band in Figure 3-2 is very similar to the bandgap in the energy-wavevector diagram for the electron state in semiconductors.

The stop band of the dispersion curve describes the strength of the interaction between the grating and the optical mode, and its magnitude is related to the coupling

coefficient κ (introduced in the next chapter) according to coupled mode theory [Yar73]:

$$\Delta\omega = \frac{2 \kappa c}{n_{eff}}$$

$$\kappa = \pi n_{eff} \frac{\Delta\lambda}{\lambda^2} \tag{3.10}$$

where c is the velocity of light in vacuum and n_{eff} the effective waveguide index for the transverse mode of interest. Equation (3.10) is used in Chapter IV to verify the accuracy of the ray optics expression for κ.

For a second order grating with a shallow groove, $K=\beta_0$ and ka<<1, there are now three propagating waves: the forward going wave (m=0, propagation constant=β_0), the upward surface emitting wave (m=-1, propagation constant=0) and the backward diffracted wave (m=-2, propagation constant=$-\beta_0$). As a result, one can obtain a 15×15 matrix from the homogeneous system, eqs. (3.2)-(3.5) and (3.7) by neglecting all evanescent waves. Following a similar procedure, the 15×15 matrix leads to the transcendental characteristic equation:

$$I_0(p_{-1}a)\,[I_0(p_0a)\,I_0(p_{-2}a)-I_2(p_0a)\,I_2(p_{-2}a)\,]$$

$$= I_1(p_{-1}a)\,\Psi_{-2}\big\{\,I_1(p_0a)\,[I_0(p_{-2}a)-I_2(p_{-2}a)\,]\,\Psi_0$$

$$+ I_1(p_{-2}a)\,[I_0(p_0a)-I_2(p_0a)\,]\,\Psi_{-2}\big\} \tag{3.11}$$

Again eq. (3.11) is valid only for shallow groove gratings because all the higher order evanescent waves are neglected in the derivation. The Bessel functions can be approximated as polynomials for small argument:

$$I_0(u) \cong 1 + \frac{u^2}{4}$$

$$I_1(u) \cong \frac{u}{2} \qquad \text{for } u \ll 1$$

$$I_2(u) \cong \frac{u^2}{8}$$

In the next chapter, the ray optics formalism is introduced to derive closed-form expressions for the coupling coefficient κ in conventional type and shiny contact DFB laser configurations. Numerical results from the Floquet-Bloch, ray optics and other standard approaches are compared in various DFB laser configurations. The advantages and disadvantages of each approach are discussed.
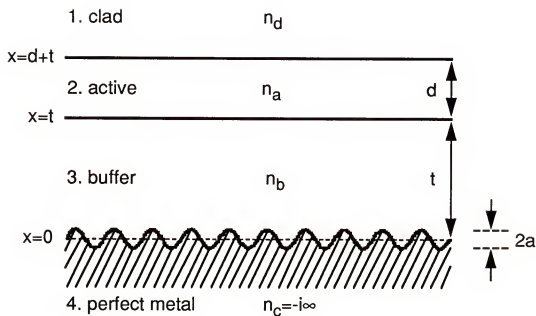
grating function: $x = f(z) = a \cdot \cos(Kz) = a \cdot \cos(2\pi z/\Lambda)$

Figure 3-1: The shiny contact DFB laser structure
used in the analysis

Figure 3-2: The ω–β_0 dispersion relation
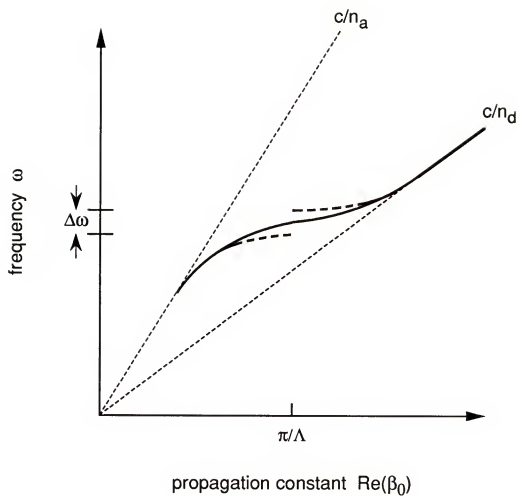for the structure shown in Figure 3-1

CHAPTER IV
RAY OPTICS APPROACH
TO THE DISTRIBUTED FEEDBACK DIODE LASER

Distributed feedback (DFB) diode lasers are key components in modern optical communication systems. In modeling laser action in these devices, one normally utilizes coupled mode theory [Kog72]. In this theory, the key laser parameter is the backward coupling coefficient κ since its magnitude determines such parameters as frequency selectivity and threshold mode gain. The standard technique to determine κ in a DFB laser is to evaluate the coupled mode integral which describes the overlap of the unperturbed mode with the grating perturbation [Str75]:

$$\kappa = \frac{k^2}{2\beta} \int \Delta n^2(x) E^2(x) dx \qquad (4.1)$$

where k is the wavevector in vacuum, β propagation constant of the waveguide mode, $\Delta n^2(x)$ index perturbation and $E(x)$ normalized electric field mode.

This technique works well for weak perturbations but shows an inherent problem as to how to choose the unperturbed waveguide geometry when the perturbation is strong [Str77, Cor88]. For a corrugated semiconductor/perfect metal interface, the coupled-mode overlap integral cannot be evaluated at all since the index perturbation is infinite

while the electric field is zero and hence the product is undefined. For a realistic semiconductor/metal or semiconductor/air grating where the index difference is large, the standard approach gives results strongly dependent on the choice of the unperturbed waveguide [Sha89].

Another widely used approach in modeling DFB lasers is the effective index transfer matrix method [Han92]. In this approach one transforms the corrugated waveguide into a stack of homogeneous layers with local effective indices. After the transformation, a standard matrix formalism from classical optics is used to model the spectral properties. For comparison with coupled-mode theory, a definition for the coupling coefficient is given [Har84]. In contrast to coupled mode theory, the transfer matrix method does not involve an unperturbed structure and hence avoids the uncertainty problem. However, there are difficulties in considering transverse modes and ambiguities in such transformations for highly asymmetrical corrugated waveguides. For example, in a simple three layer DFB waveguide with a metal clad on one side and a dielectric clad on the other side, the transfer matrix method gives exactly the same results for whether the grating is placed on the metal side or the dielectric side, i.e., such transformations do not distinguish the two different cases. Therefore one must be careful when representing a corrugated waveguide by a stack of homogeneous layers--the standard transformation should be adjusted according to some known reference.

In this chapter, a ray optics approach to the first order DFB coupling coefficient is presented, and closed-form expressions for κ are derived in DFB configurations with metalized and dielectric gratings. For standard type DFB lasers with dielectric gratings where the index difference is small, the κ values from the coupled-mode overlap integral, the transfer matrix and the ray optics methods agree very well. For a distributed Bragg reflector (DBR) type structure with a corrugated semiconductor/air interface where the index difference is larger, the κ values from the ray optics method agree with those from the transfer matrix method, but the coupled-mode overlap integral gives inconsistently smaller results depending on the choice of the unperturbed waveguide. For shiny contact DFB lasers with metalized gratings where the index difference is very large, the standard techniques do not work well and the accuracy of the ray optics expression is verified by comparing the results with those obtained using the truncated Floquet–Bloch approach explained in Chapter III. The ray optics formalism is further extended in Chapter V to deep groove configurations where the transfer matrix fails.

4.1 General Formalism

The DFB coupling coefficient κ is a measure of the backward coupling strength per unit length, so from a ray

optics point of view, κ can be expressed by the following equation [Luo90, Luo92]:

$$\kappa = B\sqrt{\eta} \qquad (4.2)$$

where B is the bounce rate for the transverse mode of interest in the planarized version of the waveguide and η the diffraction efficiency of the grating at mode bounce angle θ_{eff} (see Figure 4-1). The bounce rate is given by

$$B \equiv (2\,w_{eff}\,\tan\theta_{eff})^{-1} = \frac{\sqrt{n_a^2 - n_{eff}^2}}{2\,n_{eff}\,w_{eff}} \qquad (4.3)$$

where n_a is the refractive index of the active layer, $n_{eff}=n_a\sin\theta_{eff}$ the effective refractive index for the mode, and w_{eff} the effective waveguide thickness. The effective waveguide thickness w_{eff} is a measure of the decay of the electric field mode outside the active layer and is related to the optical confinement factor. The expression for w_{eff} can be derived directly from the definition [Tam90] for each waveguide structure, and is given in the following sections.

A closed-form expression for the diffraction efficiency can be derived for shallow grooves (ka<<1) in two ways. The first method is very similar to the truncated Floquet–Bloch approach as presented in Section 3.2. Assume a TE polarized plane wave is incident at the n_a/n_b interface at angle θ_{eff} as shown in Figure 4-1.

$$E_i = A_0\exp(-i\sigma x - i\beta z)$$

where $\beta=kn_{eff}$ is the propagation constant and $\sigma=k\sqrt{n_a^2 - n_{eff}^2}$. The reflected waves resulting from the zero and first order diffraction can be written as

$$E_r^{(0)} = a_0 \exp(i\sigma x - i\beta z)$$

$$E_r^{(-1)} = a_{-1} \exp(i\sigma x + i\beta z)$$

where the grating periodicity has been assumed to be equal to $\lambda/2n_{eff}$ since we deal with first order gratings. Neglecting higher order waves (see Section 3.2), the electric field in the incident layer n_a is then

$$E_a = E_i + E_r^{(0)} + E_r^{(-1)}$$

$$= A_0 \exp(-i\sigma x - i\beta z)$$

$$+ a_0 \exp(i\sigma x - i\beta z) + a_{-1} \exp(i\sigma x + i\beta z) \tag{4.4}$$

Similarly for layers n_b and n_c, the total electric fields can be written as

$$E_b = B_0 \exp(-px - i\beta z) + B_{-1} \exp(-px + i\beta z)$$

$$+ b_0 \exp(px - i\beta z) + b_{-1} \exp(px + i\beta z) \tag{4.5}$$

$$E_c = C_0 \exp(-qx - i\beta z) + C_{-1} \exp(-qx + i\beta z) \tag{4.6}$$

where $p=k\sqrt{n_{eff}^2 - n_b^2}$ and $q=k\sqrt{n_{eff}^2 - n_c^2}$. In eqs. (4.4)-(4.6), there are 8 unknown amplitudes relative to the incident amplitude A_0, and therefore one needs 8 independent equations (8×8 linear inhomogeneous system) in order to solve the first order diffraction efficiency:

$$\eta = \left| \frac{a_{-1}}{A_0} \right|^2 \tag{4.7}$$

Matching the boundary conditions at x=0 and x=t+f(z) results in 4 equations, each of which can be separated into two equations by setting the coefficients of exp(±iβz) to zero. Therefore a closed-form expression for η for ka<<1 can be obtained.

The second method is based on a bouncing ray picture and is physically appealing. Assume a TE polarized plane wave is incident at the n_a/n_b interface at angle θ_{eff}. Each time the ray hits the planar n_a/n_b interface, a transmitted and reflected rays are generated (denoted by t_{ab}, t_{ba} and r_{ab}, r_{ba} respectively). Each time the ray is incident at the corrugated n_b/n_c interface, there are four rays produced: $t_{bc}^{(0)}$ and $r_{bc}^{(0)}$ are the 0th order transmitted and reflected rays, and $t_{bc}^{(-1)}$ and $r_{bc}^{(-1)}$ are the 1st order transmitted and reflected rays. For shallow gratings of ka<<1, both $t_{bc}^{(-1)}$ and $r_{bc}^{(-1)}$ are much smaller than 1, and hence in the following derivation any product of two or more 1st order terms are neglected. The contribution to η includes these terms:

$$t_{ab}\cdot e^{-pt}\cdot r_{bc}^{(-1)}\cdot e^{-pt}\cdot t_{ba} = e^{-2pt}t_{ab}t_{ba}\, r_{bc}^{(-1)} \ ;$$

$$t_{ab}\cdot e^{-pt}\cdot r_{bc}^{(0)}\cdot e^{-pt}\cdot r_{ba}\cdot e^{-pt}\cdot r_{bc}^{(-1)}\cdot e^{-pt}\cdot t_{ba}$$

$$+\ t_{ab}\cdot e^{-pt}\cdot r_{bc}^{(-1)}\cdot e^{-pt}\cdot r_{ba}\cdot e^{-pt}\cdot r_{bc}^{(0)}\cdot e^{-pt}\cdot t_{ba}$$

$$=\ e^{-2pt}t_{ab}t_{ba}\, r_{bc}^{(-1)}\ \{2e^{-2pt}r_{ba}\,r_{bc}^{(0)}\}\ ;$$

. . . .

This leads to a series for η,

$$\eta = \left|\ e^{-2pt}t_{ab}t_{ba}\, r_{bc}^{(-1)}\sum_{n=0}^{\infty}(n+1)\,[e^{-2pt}r_{ba}\,r_{bc}^{(0)}]^{n}\ \right| \qquad (4.8)$$

This series is simply a derivative of a geometric series, and therefore the sum is in a simple form:

$$\sqrt{\eta} = \left| \frac{t_{ab} t_{ba} r_{bc}^{(-1)} e^{-2pt}}{(1 + r_{ab} r_{bc}^{(0)} e^{-2pt})^2} \right| \qquad (4.9)$$

Expressions for $r_{bc}^{(0)}$ and $r_{bc}^{(-1)}$ are a classical problem and can be obtained from [Mar72] for shallow sinusoidal grooves,

$$r_{bc}^{(0)} = \frac{p-q}{p+q} \qquad r_{bc}^{(-1)} = -ipa \frac{p-q}{p+q} \qquad (4.10)$$

Other transmission and reflection coefficients are written down here for reference.

$$t_{ab} = \frac{2\sigma}{\sigma - ip} \qquad t_{ba} = \frac{-2ip}{\sigma - ip}$$

$$r_{ab} = \frac{\sigma + ip}{\sigma - ip} = -r_{ba} \qquad (4.11)$$

Combining eqs. (4.9), (4.2) and (4.3), one obtains the following expression for κ,

$$\kappa = \frac{\sqrt{n_a^2 - n_{eff}^2}}{2 n_{eff} w_{eff}} \left| \frac{t_{ab} t_{ba} r_{bc}^{(-1)} e^{-2pt}}{(1 + r_{ab} r_{bc}^{(0)} e^{-2pt})^2} \right| \qquad (4.12)$$

Note that the above two methods are general for any type of cladding layer as long as the proper refractive index is used, e.g., n_c is complex for a metalized or a gain/absorption grating. It can be shown that eq. (4.7) agrees exactly with eq. (4.9) since they are both derived based on the same assumption ka<<1. This is similar to the fact that in a Fabry-Perot resonator, the wave optics and the ray optics lead to the same results.

It is interesting that the unperturbed waveguide uncertainty problem is avoided using the ray optics technique since the key parameter η is derived directly from the corrugated waveguide structure. The ray optics technique works well for strong coupling as well as weak coupling DFB configurations, and it also provides device designers with simple expressions for κ which are much easier to implement than the standard overlap integral programs since they can be evaluated without using numerical techniques of any kind (see Section 4.3). In addition, the ray optics technique is physically intuitive and gives one a different perspective on how DFB lasers actually work. In the following sections the ray optics technique is applied to several conventional and nonconventional, including the shiny contact DFB laser configurations.

4.2 DFB Lasers with Metalized Gratings

In this section, we show how to derive an accurate closed-form expression for κ for the shiny contact DFB waveguide shown in Figure 3-1 despite the complexity of such structures. The approach we use to demonstrate the accuracy of the ray optics technique is to compare ray optics and Floquet-Bloch derived plots of κ for perfect metal grating (see Chapter III). We then show that the ray optics plots change very little when the perfect metal is replaced by a shiny metal such as gold.

A perfect metal is by definition a metal whose conductivity is infinite, i.e., its complex refraction index $n_c = -i\infty$. In this case $q = \infty$, $r_{bc}^{(0)} = -1$ and $r_{bc}^{(-1)} = ipa$, and $\sqrt{\eta}$ and w_{eff} are

$$\sqrt{\eta} = \frac{(ka)\sqrt{n_a^2 - n_{eff}^2}(n_{eff}^2 - n_b^2)}{(n_a^2 - n_{eff}^2)\sinh^2(pt) + (n_{eff}^2 - n_b^2)\cosh^2(pt)}$$

$$w_{eff} = d + \frac{1}{p}\frac{(p^2 + \sigma^2)\tanh(pt) - \sigma^2 pt/\cosh^2(pt)}{p^2 + \sigma^2\tanh^2(pt)} + \frac{1}{s}$$

$$\cong d + \frac{1}{p}\tanh(pt) + \frac{1}{s}$$

where $s = k\sqrt{n_{eff}^2 - n_d^2}$. The coupling coefficient is then, from eq. (4.12),

$$\kappa = \frac{ka(n_a^2 - n_{eff}^2)(n_{eff}^2 - n_b^2)}{2n_{eff}w_{eff}[(n_a^2 - n_{eff}^2)\sinh^2(pt) + (n_{eff}^2 - n_b^2)\cosh^2(pt)]} \qquad (4.13)$$

This equation is useful since it depends only on the wavelength, the groove depth and the parameters of the planar waveguide structure. Therefore, once the eigenvalue equation of the planar waveguide is solved, the magnitude of the coupling coefficient can be calculated in a straightforward manner. Strictly speaking, this equation is valid only for $ka \ll 1$ because of the assumption needed in deriving the expression for the diffraction efficiency. However, as indicated by Rigrod and Marcuse [Rig76], expressions of this type are in most cases at least qualitatively correct for ka values well beyond the $ka \ll 1$ limit used in the derivation.

In the real world, perfect metals are closely approximated by "shiny metals," i.e., those metals with a big

extinction coefficient. Gold is one such shiny metal at wavelength of 0.85μm since its extinction index is much greater than its refractive index (n_c=0.16-i5.3). For such realistic metals, one can simply use eq. (4.13) with the proper complex refractive index.

As a first example, Figure 4-2 shows a plot of κ vs. ka for the AlGaAs corrugated double heterostructure. It is observed that for perfect metal gratings, the ray optics and the Floquet-Bloch curves agree very well at small values of ka, deviating by only 10% at ka=1. The dashed line (for gold) follows the solid line (for perfect metal) closely as expected. In Figure 4-3 we plot the coupling coefficient versus the thickness of the buffer layer t. Both approaches are well consistent over the whole range of t. The roll-over behavior is attributed to the fact that as t becomes very small, the mode is pushed far away from the grating where the interaction takes place, causing the mode overlap to decrease as t is reduced further. In Figure 4-4 the coupling coefficient is plotted versus the thickness of the active layer d, with t as a parameter. Excellent agreement between the two approaches is observed again.

The above derivation is based on gratings of a sinusoidal shape. For other grating tooth shape, the coupling coefficient should be multiplied by a geometric factor G: G=1 for sinusoidal gratings, G=8/π^2 for triangular gratings and G=4/π for square gratings. This factor comes

from the Fourier coefficients in the derivation of the
diffraction efficiency.

4.3 DFB Lasers with Dielectric Gratings

In this section, we apply the ray optics technique to a
generic 5-layer separate confinement heterostructure (SCH)
DFB laser (see Figure 4-5(a)), and show how to utilize the
ray optics expression to compute κ in a more complex,
multiquantum well (MQW) DFB configuration (see Figure 4-
5(b)). Then the results from the ray optics expression are
compared with published values of κ determined by the
standard overlap integral and transfer matrix techniques.

The effective waveguide thickness w_{eff} for the 5-layer
SCH structure is given as

$$
\begin{aligned}
w_{eff} &= d + \frac{(\sigma^2-\rho^2) X Y + \sigma^2\rho(\rho^2+q^2)(t+1/q)}{\rho(\sigma^2 X^2 + \rho^2 Y^2)} \\
&\quad + \frac{(\sigma^2-\rho'^2) X'Y' + \sigma^2\rho'(\rho'^2+q'^2)(t'+1/q')}{\rho'(\sigma^2 X'^2 + \rho'^2 Y'^2)} \\
&\equiv d + t + t' + \frac{1}{q} + \frac{1}{q'}
\end{aligned}
$$

where

$$
\sigma = k\sqrt{n_a^2 - n_{eff}^2}
$$

$$
\rho = k\sqrt{n_b^2 - n_{eff}^2} \qquad\qquad \rho' = k\sqrt{n_b'^2 - n_{eff}^2}
$$

$$
q = k\sqrt{n_{eff}^2 - n_c^2} \qquad\qquad q' = k\sqrt{n_{eff}^2 - n_c'^2}
$$

$$
X = \rho\cos(\rho t) + q\sin(\rho t) \qquad X' = \rho'\cos(\rho't') + q'\sin(\rho't')
$$

$$Y = \rho\sin(\rho t) - q\cos(\rho t) \qquad Y' = \rho'\sin(\rho't') - q'\cos(\rho't')$$

After manipulation, eq. (4.9) leads to

$$\sqrt{\eta} = G \frac{a\sigma\rho^2(\rho^2+q^2)}{\sigma^2 X^2 + \rho^2 Y^2}$$

$$= G \frac{a\sigma\rho^2(\rho^2+q^2)}{\sigma^2[\rho\cos(\rho t)+q\sin(\rho t)]^2 + \rho^2[\rho\sin(\rho t)-q\cos(\rho t)]^2}$$

where G is the geometric factor depending on the groove shape of the grating: G=1 for a sinusoidal grating, $G=8/\pi^2$ for a triangular grating and $G=4/\pi$ for a square grating. The coupling coefficient κ is then

$$\kappa = G \frac{ka(n_a^2-n_{eff}^2)\rho^2(\rho^2+q^2)}{2\,n_{eff}w_{eff}(\sigma^2 X^2+\rho^2 Y^2)} \qquad (4.14)$$

$$= G \frac{ka(n_a^2-n_{eff}^2)\rho^2(\rho^2+q^2)}{2n_{eff}w_{eff}\{\sigma^2[\rho\cos(\rho t)+q\sin(\rho t)]^2 + \rho^2[\rho\sin(\rho t)-q\cos(\rho t)]^2\}}$$

As mentioned above, eq. (4.14) is valid only for ka<<1 because of the approximations made in deriving η. However, as indicated by Rigrod and Marcuse [Rig76], expressions of this type are in most cases at least qualitatively correct for ka values well beyond the limit used in the derivation.

To use eq. (4.14) to determine κ in an MQW DFB laser structure as shown in Figure 4-5(b), one needs to transform the MQW structure into an equivalent SCH structure by replacing the quantum well/barrier layers by a single homogeneous layer with an r.m.s. refractive index n_a [Sam90],

$$n_a^2 = \frac{N_{qw}d_{qw}n_{qw}^2 + N_{br}d_{br}n_{br}^2}{N_{qw}d_{qw} + N_{br}d_{br}} \qquad (4.15)$$

where N_{qw}, N_{br}, d_{qw}, d_{br}, n_{qw} and n_{br} are the numbers, thicknesses and refractive indices of the quantum well and barrier layers respectively.

The formula for κ, eq. (4.14), is easy to use since it depends only on the wavelength, the grating amplitude and shape, and parameters of the planar waveguide geometry. Therefore, once the effective index n_{eff} of the planar waveguide is obtained, the magnitude of the coupling coefficient can be calculated in a straightforward manner. Since the accuracy for n_m is not critical in the ray optics computation, one can use an approximate method to estimate n_m without solving the transcendental eigenvalue equation. For example, in most laser structures, $n_c = n_c'$ and the thickness of the inner layers is small compared with the wavelength. Therefore, one can transform the SCH or MQW waveguide into a simple 3 layer waveguide using a technique similar to eq. (4.15), i.e., all the inner layers are regarded as a single homogeneous layer with an r.m.s. refractive index n_e and thickness d_e. In this case, n_e and d_e are given by

$$n_e^2 = \frac{d\,n_a^2 + t\,n_b^2 + t'n_b'^2}{d + t + t'} \tag{4.16}$$

$$d_e = d + t + t' \tag{4.17}$$

and the following closed-form expression for n_{eff} for such a symmetric 3-layer waveguide can be used [Che83],

$$n_{eff}^2 = n_e^2 - \frac{2}{k^2 d_e^2}\,\ln\,[1 + \frac{k^2 d_e^2}{2}(n_e^2 - n_c^2)\,] \tag{4.18}$$

There are also formulas for asymmetric 3-layer waveguides ($n_c \neq n_c^!$) in [Bot83] and the references. With the help of these formulas, the ray optics technique provides the means for quick estimates of κ in relatively complex DFB configurations without using numerical techniques of any kind.

The above derivation is written for $n_{eff} < n_b$ and $n_{eff} < n_b^!$, i.e., the transverse components of the two counter running waves in the guiding layers are traveling waves. In case they are evanescent, i.e., $n_{eff} > n_b$ and $n_{eff} > n_b^!$, then ρ and ρ' should be replaced by $-ik\sqrt{n_{eff}^2 - n_b^2}$ and $-ik\sqrt{n_{eff}^2 - n_b^2}$ respectively.

As a first example, we plot κ versus ka in Figure 4-6 for a typical 1.55μm symmetric SCH DFB laser [Sak82]. It is clear that the ray optics expression eq. (4.14) virtually reproduces the curve obtained using numerical integration. If one uses eq. (4.18) to estimate n_{eff}, one obtains κ values with an error of about 1%. It is interesting to note that the linear dependence of κ on ka is explicit in eq. (4.14). In the standard numerical approach, one must do a number of integrations and plot the data properly before the linear dependence becomes obvious. The second example Figure 4-7 is a plot of κ versus the thickness of the active layer d for the 4-layer structure shown by Itaya et al. [Ita84]. Excellent agreement between the two approaches is observed over the whole range of interest. Using eq. (4.18) to estimate n_{eff} for eq. (4.14), one gets better than 1% accuracy

for κ when t≤0.2μm and d≤0.3μm. For t=0.3μm, the error increases to about 5% at d=0.2μm, and is even larger for d>0.2μm. However, the region where d is large is usually of little interest to DFB laser designers since threshold current increases as d increases. The roll-over behavior for t=0.1μm has to do with the fact that B has a maximum at some value of d and $\sqrt{\eta}$ increases monotonically with decreasing d due to the monotonic decrease in θ_{eff}. Since κ is given by B$\sqrt{\eta}$, there will be a peak in κ near this d value. Similar phenomena also occur in metalized DFB laser configurations in Figure 4-3. In the next example Figure 4-8, κ is plotted versus the number of quantum wells for a 1.55μm MQW DFB laser as shown by Makino and Adams [Mak91]. The ray optics, coupled mode and transfer matrix approaches show excellent agreement for such a weak perturbation. In this MQW structure, eq. (4.18) can be used for n_{eff} in the ray optics expression without introducing any noticeable error (much less than 1%). It is interesting to note that there is a value for N_w which maximizes κ (for the present case, N_w=2). This is also similar to the roll-over behavior in Figure 4-7. As the final example, Figure 4-9 is a plot for κ in a DBR type structure with a corrugated semiconductor/air interface where the perturbation is stronger. The ray optics formula agrees with the transfer matrix method very good in this case. Note that the superlinear behavior is because the t is assumed to be reduced when the grating is deeper. The coupled mode results are inconsistently underestimated by

about 20-30% at only ka=0.2, depending on the choice of the unperturbed structure: the lower dotted curve is based on a 4-layer unperturbed waveguide where the the n_b/n_c interface is in the center, and the upper dash-dot curve is based on a 5-layer unperturbed waveguide where an additional "grating layer" is assumed with an averaged refractive index.

4.4 Mixed Gain/Index Coupled Gratings

So far the coupling coefficient has been assumed to be real and only the magnitude of κ has been calculated. In the most general case, the cladding layer may be lossy due to free carrier or band-to-band absorption when a metal or a small bandgap material is used. In such cases κ becomes complex. A complex κ can in principle improve the single frequency yield [Kap82]. The complex coupling coefficient should be written as

$$\kappa = \kappa_i + i\kappa_g = |\kappa| \, e^{i\phi} \qquad (4.19)$$

where κ_i and κ_g denote the index and gain (or loss) coupling. For practical cases with loss gratings, $\kappa_i \gg \kappa_g$ and $\kappa_i \cong |\kappa|$ since one does not want too much loss which increases the threshold current. Under this condition, the analysis presented in previous sections can be used to calculate $|\kappa|$, and κ_g can be computed in two ways.

The first method is to obtain $|\kappa|$ from eq. (4.12) using proper complex refractive indices. Then the magnitude of κ_g relative to κ_i is determined from the ratio of the imaginary

part to the real part of the complex index perturbation Δn^2 for the grating in accordance with the coupled mode definition eq. (4.1).

The second method is to define a complex amplitude diffraction efficiency similar to eq. (4.9) but without the absolute value. Then complex κ is expressed as

$$\kappa = \frac{\sqrt{n_a^2 - n_{eff}^2}}{2\, n_{eff}\, w_{eff}} \left[\frac{t_{ab} t_{ba}\, r_{bc}^{(-1)}\, e^{-2pt}}{(1 + r_{ab}\, r_{bc}^{(0)}\, e^{-2pt})^2} \right] \qquad (4.20)$$

Since eq. (4.20) always gives a complex number even for a pure index coupling structure, one has to find the reference phase before determining the actual phase ϕ of the complex coupling coefficient. Assuming the loss is small, one first turns off the loss term by setting the extinction index to zero (for dielectric) or infinity (for metal) and gets κ_0

$$\kappa_0 = |\kappa_0| \exp(i\phi_0)$$

Then one turns on the loss term and gets κ_1

$$\kappa_1 = |\kappa_1| \exp(i\phi_1)$$

Finally the complex coupling coefficient is

$$\kappa = |\kappa_1| \exp(i\phi_1 - i\phi_0) \qquad (4.21)$$

A properly controlled loss coupling DFB mechanism has been shown to improve the single frequency yield [Tsa92]. In the shiny contact DFB laser, the loss coupling can be controlled by the metalization process since the shiny metal (gold) is almost lossless. For example, thin layers of titanium and platinum can be deposited first on the corrugated semiconductor for better p-contact reliability. Since titanium is lossy and not a shiny metal, this layer

gives rise to periodic loss modulation. Alternatively, a thin contact layer of heavy doping may be grown on top of the cladding layer for better electrical resistance. The free carrier or band-to-band absorption in this contact layer introduces a loss coupling DFB mechanism. Optimization of these layer thicknesses, which can be done using the extended ray optics approach, should lead to DFB lasers of high reliability and high single frequency yield.
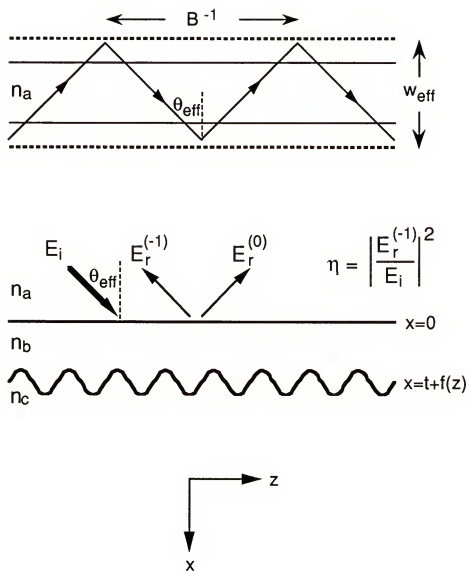
Figure 4-1: Diagram for the ray optics calculations of κ
for a generic DFB laser structure
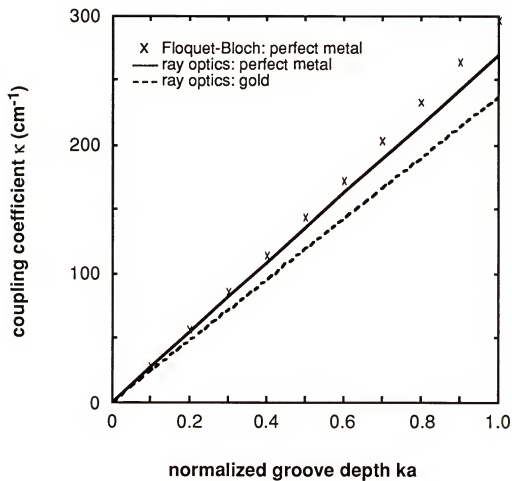
Figure 4-2: The coupling coefficient for the DFB laser
in Figure 3-1 with the following parameter values:
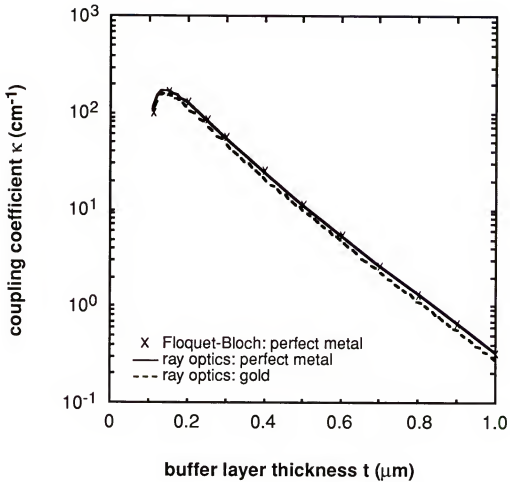$\lambda=0.85\mu m, d=0.1\mu m, t=0.3\mu m, n_a=3.6, n_b=3.4, n_d=3.4$

Figure 4-3: The coupling coefficient for the DFB laser
in Figure 3-1 with the following parameter values:
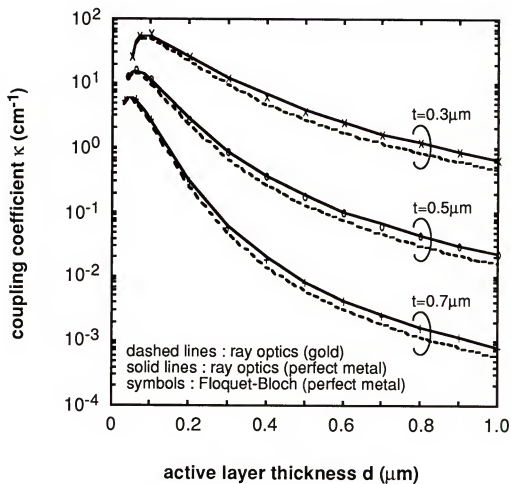$\lambda=0.85\mu m, d=0.1\mu m, ka=0.2, n_a=3.6, n_b=3.4, n_d=3.4$

Figure 4-4: The coupling coefficient for the DFB laser
in Figure 3-1 with the following parameter values:
$\lambda = 0.85\mu m, ka = 0.2, n_a = 3.6, n_b = 3.4, n_d = 3.4$
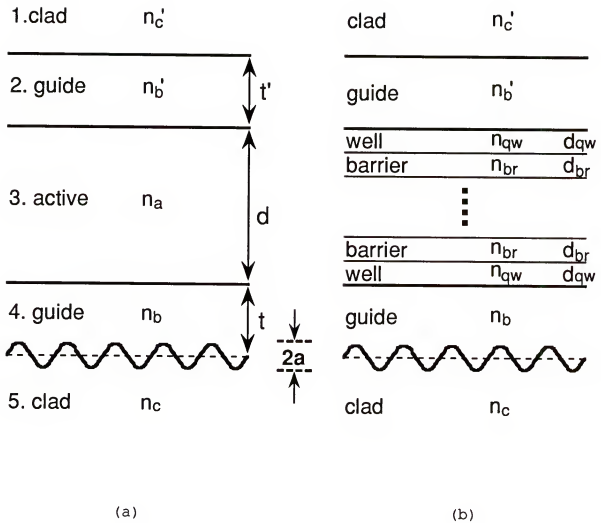
Figure 4-5: Generic DFB structure with dielectric gratings
    (a) SCH DFB laser configuration
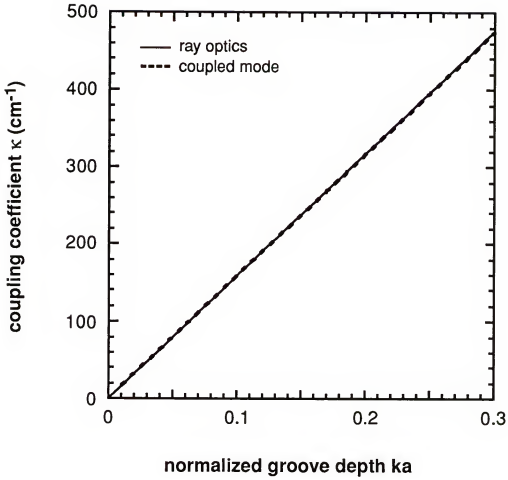   (b) MQW DFB laser configuration

Figure 4-6: The coupling coefficient for the SCH DFB laser
in Figure 4-5(a) for sinusoidal gratings
with the following parameter values:
$n_a=3.54, n_b=n_b'=3.40, n_c=n_c'=3.17$
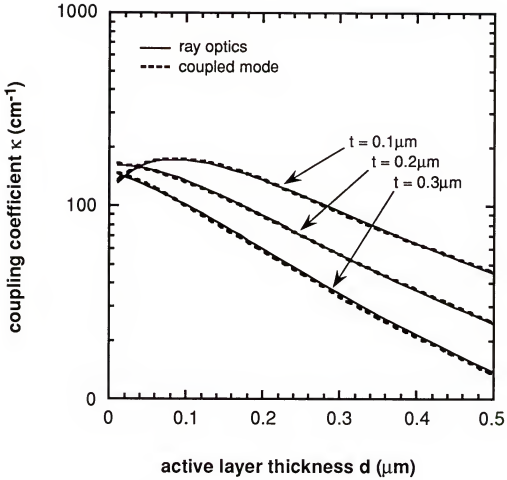$\lambda=1.55\mu m, d=0.1\mu m, t=t'=0.1\mu m$

Figure 4-7: The coupling coefficient for the SCH DFB laser
in Figure 4-5(a) for sinusoidal gratings
with the following parameter values:
$n_a=3.54, n_b=3.39, n_c=n_c'=3.17$
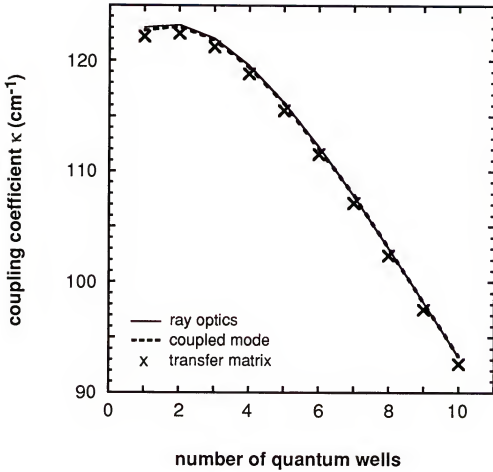$\lambda=1.55\mu m, t'=0, 2a=500\text{Å}$

Figure 4-8: The coupling coefficient for the MQW DFB laser
in Figure 4-5(b) for square gratings
with the following parameter values:
$n_{qw}=3.57, n_{br}=3.39, n_b=n_b'=3.39, n_c=n_c'=3.17$
$d_{qw}=70\text{Å}, d_{br}=100\text{Å}, t=0.185\mu m, t'=0.01\mu m$
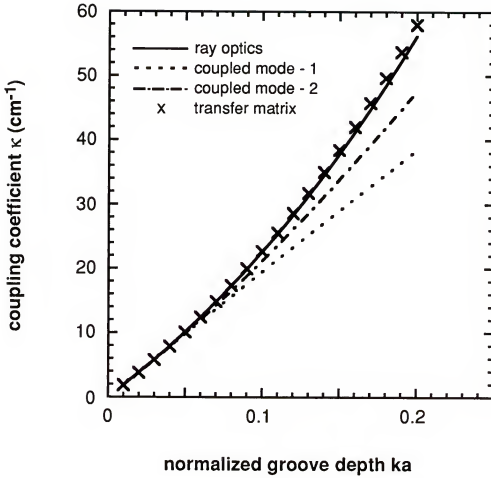$\lambda=1.55\mu m, 2a=300\text{Å}$

Figure 4-9: The coupling coefficient for a DBR structure with square gratings and the following parameter values: $\lambda=7.8\mu m, d=1\mu m, t+a=1\mu m, t'=0, n_a=5.0, n_b=4.7, n_c=1.0, n_c'=4.7$

CHAPTER V
DEEP GROOVE GRATINGS

In previous chapters, only shallow groove gratings (ka<<1) have been considered in the analysis. Such gratings are commonly utilized in DFB lasers in fiber communication applications. In this chapter, we discuss the theoretical aspects of deep groove gratings and propose a grating surface emitter (GSE) structure with a deep groove metalized grating. This shiny contact GSE structure can be potentially fabricated into two dimensional arrays of low threshold current, single frequency devices competitive with vertical cavity surface emitting lasers (VCSEL) [Jew91]. In Section 5.1, the formalism for the diffraction efficiency for deep groove gratings is outlined using the Rayleigh approach. Then numerical results for first and second order gratings are given in Sections 5.2 and 5.3, and the design of such potential GSE devices discussed.

5.1 General Formalism

In this section, the shiny contact DFB laser as shown in Figure 5-1 is discussed. This DFB structure is similar to the one drawn in Figure 3-1 except for arbitrary groove depth. Assume the cladding layer is made of sinusoidally

74

corrugated perfect metal and we consider TE modes, i.e., the electric field is y-oriented. Recall the ray optics definition for the coupling coefficient κ in Chapter IV,

$$\kappa = B\sqrt{\eta} = \frac{\sqrt{n_a^2 - n_{eff}^2}}{2\, n_{eff}\, w_{eff}}\,\sqrt{\eta} \tag{5.1}$$

Now we show how to compute the diffraction efficiency η for a grating with depth comparable to or even larger than the wavelength (ka~1). As mentioned in Chapter III, even though the Rayleigh assumption is questionable for the general case, the approach itself is straightforward and can provide fast and accurate results for sinusoidal gratings compared with other techniques [Pet80]. Therefore we use the Rayleigh expansion in this chapter.

Assume the incident wave has unit amplitude and x- and z-propagation constant σ_0 and β_0 respectively ($\beta_0 = n_{eff}k$):

$$\exp(i\sigma_0 x)\exp(-i\beta_0 z)$$

Then the total electric field in layers n_a and n_b can be expressed as, according to Rayleigh assumption,

$$E_a(x,z) = \exp(i\sigma_0 x)\exp(-i\beta_0 z) + \sum_{m=-\infty}^{\infty} A_m\exp(-i\sigma_m x)\exp(-i\beta_m z)$$

$$E_b(x,z) = \sum_{m=-\infty}^{\infty} [B_m\exp(-p_m x)+C_m\exp(p_m x)]\exp(-i\beta_m z)$$

$$E_c(x,z) = 0 \text{ in the perfect metal} \tag{5.2}$$

where

$$\beta_m = \beta_0 + mK = \beta_0 + m(2\pi/\Lambda) \qquad \Lambda: \text{ grating periodicity}$$
$$\sigma_m = \sqrt{n_a^2 k^2 - \beta_m^2} \text{ or } -i\sqrt{\beta_m^2 - n_a^2 k^2}$$

$$p_m = \sqrt{\beta_m{}^2 - n_b{}^2 k^2}$$

$$k = 2\pi/\lambda \qquad\qquad \lambda: \text{wavelength in vacuum}$$

Care should be taken for the sign of σ_m. The former expression is used for $n_a > n_{eff}$ and the latter for $n_a < n_{eff}$. Following a boundary matching procedure similar to that presented in Section 3.1, the infinite inhomogeneous linear system is so obtained,

$$A_0 \exp(-i\sigma_0 t) - B_0 \exp(-p_0 t) - C_0 \exp(p_0 t) = -\exp(i\sigma_0 t)$$

$$i\sigma_0 A_0 \exp(-i\sigma_0 t) - p_0 B_0 \exp(-p_0 t) + p_0 C_0 \exp(p_0 t) = i\sigma_0 \exp(i\sigma_0 t)$$

$$A_m \exp(-i\sigma_m t) - B_m \exp(-p_m t) - C_m \exp(p_m t) = 0 \qquad\qquad \forall m \neq 0$$

$$i\sigma_m A_m \exp(-i\sigma_m t) - p_m B_m \exp(-p_m t) + p_m C_m \exp(p_m t) = 0 \qquad\qquad \forall m \neq 0$$

$$\sum_{m=-\infty}^{\infty} [(-1)^{m-n} B_m I_{m-n}(p_m a) + C_m I_{m-n}(p_m a)] = 0 \qquad\qquad \forall n$$

$$(5.3)$$

where I_n is the modified (or hyperbolic) Bessel function of the first kind (of order n). This system can be solved using standard numerical techniques, and the results for two special cases are given below.

5.2 <u>First Order Deep Groove Gratings</u>

For a first order grating, $K = 2\beta_0$ or $\Lambda = \lambda/(2n_{eff})$, there are two traveling terms that carry electromagnetic power: the fundamental forward wave (m=0, amplitude A_0, propagation constant β_0) and the backward diffracted wave (m=-1, amplitude A_{-1}, propagation constant $-\beta_0$). The diffraction

efficiency is then $\eta = |A_{-1}|^2$, and numerical data for the coupling coefficient κ can be obtained from eq. (5.1).

In order to see how many terms are required for the Rayleigh expansion eq. (5.2) to converge, κ is plotted in Figure 5-2 versus the number of terms in the expansion for ka=0.5 using the parameter set as in Figure 4-2. From this figure it is obvious that about 10 terms are needed for a stable and convergent output, and this corresponds to a 30×30 matrix. Then we plot the results for κ versus ka in Figure 5-3 for the same structure, where the solid curve is obtained using the numerical data for η from an expansion of at least 10 terms, dashed line from the closed-form expression eq. (4.13) based on a two wave approximation, and the dotted line from the transfer matrix method. It is observed that for small values of ka, there is no significant difference among these three curves. For larger values of ka, however, the accurate results should be sublinear and then rolling over. The two wave approximated eq. (4.13) produces linear results while the transfer matrix goes super linear. This indicates that the ray optics formalism is superior: for best accuracy, one can use numerical data for η, and for simplicity, one can use the closed-form expression which is still better than the other techniques.

The results in this section show that for a first order grating, κ does not always go up when the groove depth increases. Therefore one has to be careful in maximizing κ using a deep groove device. There is an optimal value of the

groove depth for maximum diffraction efficiency. Similar behavior for the diffraction efficiency of a corrugated air/metal grating has been reported in the literature using other techniques such as [Moh86].

5.3 Second Order Deep Groove Gratings

For a second order grating, $K=\beta_0$ or $\Lambda=\lambda/n_{eff}$, the basic three terms are $m=0$, $m=-1$ and $m=-2$ whose z-propagation constants are β_0, 0 and $-\beta_0$ respectively. The first order diffracted wave A_{-1} corresponds to the surface emitting beam and the second order diffracted wave A_{-2} provides the backward coupling. In a low threshold GSE design when low surface emitting power is needed, one wants to maximize A_{-2} but minimize A_{-1} since A_{-2} provides the feedback but A_{-1} is the radiation loss to the laser cavity. Such a design can not be realized using simplified theories valid only for shallow groove gratings. For example, when higher order waves are neglected, A_{-2} is always much less than A_{-1} [Rig76], consequently conventional GSE lasers using shallow groove gratings show high threshold current while produce high surface emitting power, and this is why they have not been utilized in low threshold, low power applications such as chip-to-chip communications.

In this section we investigate deep groove effects in second order metalized gratings by including those higher order evanescent waves in the ray optics formalism. The

results presented in this section will shed light on potential low threshold GSE lasers which could be competitive with VCSELs [Tak92].

Because the grating wavevector is smaller in the second order grating, higher order waves do not decay as fast as in the first order case. We find that about 15 terms are required for convergent results, and this corresponds to a 45×45 matrix. Both $|A_{-1}|$ and $|A_{-2}|$ are plotted in Figure 5-4 for the same configuration as in Figure 5-3 except for the second order grating. In the region ka<0.5, $|A_{-1}|$ is much larger than $|A_{-2}|$ as expected, and a large portion of the optical power is emitted as surface radiation loss. For high power GSE lasers where the threshold is less concerned, a large $|A_{-1}|$ is desired for large surface emitting power. For low threshold GSE or edge emitting DFB lasers, however, a large $|A_{-2}|$ for the feedback and a small $|A_{-1}|$ for low radiation loss are preferred. This cannot be achieved using shallow groove gratings, so most people do not use second order gratings for edge emitting DFB lasers even though the single frequency yield is better [Car92]. When the groove depth becomes bigger, $|A_{-1}|$ starts to roll over while $|A_{-2}|$ keeps rising. At around ka=1, $|A_{-1}|$ is much less than $|A_{-2}|$, and this is the region of interest for such a novel low threshold GSE or DFB laser. For a low power GSE laser, one can in principle achieve threshold currents as low as for conventional DFB lasers. For a DFB laser using second order

deep groove gratings, one should be able to demonstrate high single frequency yield and easy fabrication.

The oscillatory behavior in Figure 5-4 using the Rayleigh expansion shows agreement with the diffraction of a corrugated air/metal interface using other techniques [Moh86]. We have also observed in our laboratory a similar phenomenon that high order waves are brighter than the low order ones when the grating depth is comparable to or larger than the wavelength. Therefore, it is believed that such GSE lasers using deep groove shiny contact gratings can be realized with a proper design. Due to the superior thermal properties inherent in such deep groove shiny contact GSE laser structures, they could be competitive with vertical cavity surface emitting lasers in future chip-to-chip communication technologies.
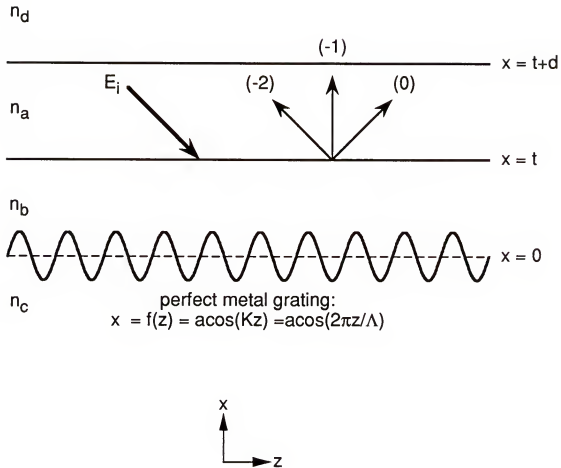
Figure 5-1: Diagram for the ray optics calculations of κ
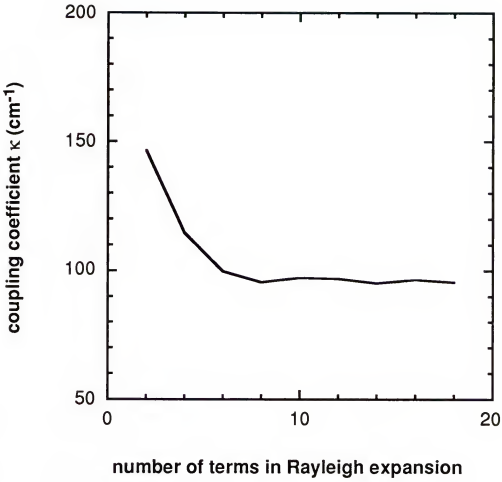for a generic DFB laser structure

number of terms in Rayleigh expansion

Figure 5-2: The coupling coefficient for the DFB structure
in Figure 5-1 and the following parameter values:
$\lambda=0.85\mu m$, $d=0.1\mu m$, $t=0.3\mu m$, $ka=0.5$
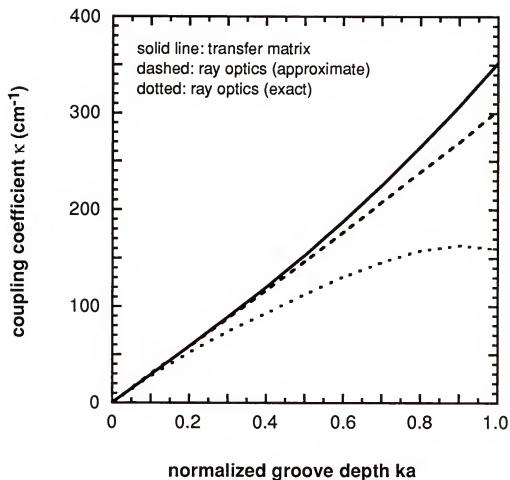$n_a=3.6$, $n_b=3.4$, $n_c=-i\infty$, $n_d=3.4$

Figure 5-3: The coupling coefficient for the DFB structure
in Figure 5-1 and the following parameter values:
$\lambda=0.85\mu m$, $d=0.1\mu m$, $t=0.3\mu m$,
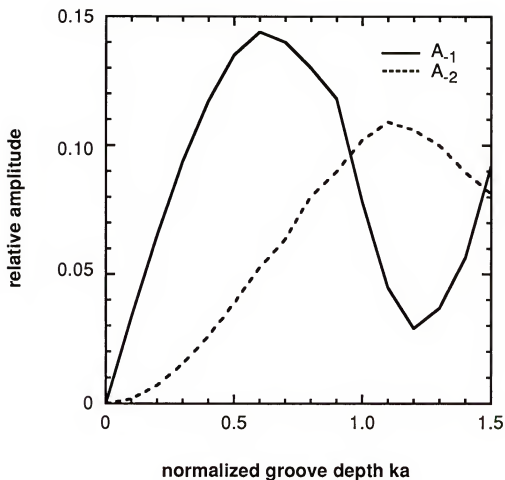$n_a=3.6$, $n_b=3.4$, $n_c=-i\infty$, $n_d=3.4$

Figure 5-4: The relative amplitude for two diffraction orders
of a second order DFB structure with these parameter values:
$\lambda=0.85\mu m$, $d=0.1\mu m$, $t=0.3\mu m$, $n_a=3.6$, $n_b=3.4$, $n_d=3.4$

CHAPTER VI
CONCLUSIONS AND RECOMMENDATIONS

In conclusion, shiny contact diode lasers have been demonstrated for the first time in the 1.3μm InGaAsP/InP material system. Power levels greater than one watt pulsed have been achieved at room temperature, among the highest for DH InGaAsP/InP lasers and comparable to those obtained from state-of-the-art separate confinement heterostructure single quantum well lasers. The experimental data have been successfully explained by the theory and key parameters determined from the measurements. Using measured parameters, improvements in continuous wave performance levels relative to conventional devices are predicted. We believe that these improvements can be realized according to our optimal design, and it is recommended for future research.

The advantages of combining the shiny contact with the DFB laser structure have been made clear. Ray optics and Floquet-Bloch formalisms have been developed to model the lasing properties of these shiny contact DFB lasers as well as conventional DFB lasers. It has been shown that in standard type DFB lasers with dielectric gratings where the index difference is small, the κ values from the coupled mode overlap integral, the transfer matrix method and the ray optics expression agree very well. In shiny contact DFB

lasers with metalized gratings where the index difference is very large, the standard techniques do not work well and the ray optics expression is consistent with the Floquet-Bloch approach. The ray optics formalism has been extended to investigate deep groove effects of second order metalized gratings. Our calculations indicate that low threshold grating surface emitting laser arrays are possible by the use of deep groove shiny contact gratings. GSE arrays of this type could be competitive with vertical cavity surface emitting laser arrays due to their superior thermal properties.

For future research, the shiny contact DFB laser structure with the loss coupling mechanism mentioned in Chapter IV offers several advantages absent in conventional DFB lasers. We believe that it is worthwhile to make such devices in the InGaAsP/InP system since the key technology, fabrication of the shiny contact, has been realized in this dissertation. The low threshold GSE laser array using deep groove shiny contact gratings, first proposed in this study, is also very interesting. Experimental verification of such devices could have a potential impact on future chip-to-chip communication technologies.

REFERENCES

[Agr86]   G. P. Agrawal and N. K. Dutta, *Long-Wavelength Semiconductor Lasers*, New York: Van Nostrand, 1986.

[Asa81]   M. Asada, A. R. Adams, K. E. Stukjaer, Y. Suematsu, Y. Itaya and S. Arai, "The temperature dependence of the threshold current of GaInAsP/InP DH lasers," *IEEE J. Quantum Electron.*, vol. QE-17, pp. 611-619, 1981.

[Asa83]   M. Asada and Y. Suematsu, "The effects of loss and nonradiative recombination on the temperature dependence of threshold current in 1.5-1.6μm GaInAsP/InP lasers," *IEEE J. Quantum Electron.*, vol. QE-19, pp. 917-923, 1983.

[Beh90]   A. Behfar-Rad, J. R. Shealy, S. R. Chinn and S. S. Wong, "Effect of cladding layer thickness on the performance of GaAs-AlGaAs graded index separate confinement heterostructure single quantum well lasers," *IEEE J. Quantum Electron.*, vol. QE-26, pp. 1476-1480, 1990.

[Bot84]   D. Botez, "The effect of carrier-induced index depressions on fundamental-transverse-mode characteristics in DH laser structures," *RCA Review*, vol. 45, pp. 23-32, 1984.

[Cas78]   H. C. Casey and M. B. Panish, *Heterostructure Lasers*, New York: Academic, 1978.

[Che83]   K. L. Chen and S. Wang, "An approximate expression for the effective refractive index in symmetric DH lasers," *IEEE J. Quantum Electron.*, vol. QE-19, pp. 1354-1356, 1983.

[Cor88]   P. Correc, "Coupling coefficients for trapezoidal gratings," *IEEE J. Quantum Electron.*, vol. QE-24, pp. 8-10, 1988.

[Dut82]   N. K. Dutta and R. J. Nelson, "The case for Auger recombination in $In_{1-x}Ga_xAs_yP_{1-y}$," *J. Appl. Phys.*, vol. 53, pp. 74-92, 1982.

[Han92]   S. Hansmann, "Transfer matrix analysis of the spectral properties of complex distributed feedback laser structures," *IEEE J. Quantum Electron.*, vol. QE-28, pp. 2589-2595, 1992.

[Har84]   A. Hardy, "Exact derivation of the coupling coefficient in corrugated waveguides with rectangular tooth shape," *IEEE J. Quantum Electron.*, vol. QE-20, pp. 1132-1139, 1984.

[Hen79]   C. H. Henry, P. M. Petroff, R. A. Logan and F. R. Merritt, "Catastrophic damage of $Al_xGa_{1-x}As$ double-heterostructure laser material," *J. Appl. Phys.*, vol. 50, pp. 3721-3732, 1979.

[Ita84]   Y. Itaya, T. Matsuoka, K. Kuroiwa and T. Ikegami, "Longitudinal mode behaviors of 1.5μm range GaInAsP/InP distributed feedback lasers," *IEEE J. Quantum Electron.*, vol. QE-20, pp. 230-235, 1984.

[Jew91]   J. L. Jewell, J. P. Harbison, A. Scherer, Y. H. Lee and L. T. Florez, "Vertical-cavity surface-emitting lasers: design, growth, fabrication, characterization," *IEEE J. Quantum Electron.*, vol. QE-27, pp. 1332-1346, 1991.

[Kap82]   E. Kapon, A. Hardy and A. Katzir, "The effect of complex coupling coefficient on distributed feedback lasers," *IEEE J. Quantum Electron.*, vol. QE-18, pp. 66-71, 1982.

[Kat92]   A. Katz, ed., *Indium Phosphide and Related Materials: Processing, Technology, and Devices*, Boston: Artech House, 1992.

[Kog72]   H. Kogelnik and C. V. Shank, "Coupled-wave theory of distributed feedback lasers," *J. Appl. Phys.*, vol. 43, pp. 2327-2335, 1972.

[Kre77]   H. Kressel and J. K. Butler, *Semiconductor Lasers and Heterostructure LEDs*, New York: Academic, 1977.

[Lie91]   S. K. Liew, N. W. Carson, D. P. Bour, G. A. Evans, and E. Van Gieson, "Demonstration of InGaAs/AlGaAs strained-layer distributed-feedback grating-surface-emitting lasers with a buried second-order grating structure," *Appl. Phys. Lett.*, vol. 58, pp. 228-230, 1991.

[Luo90]   H. J. Luo and P. S. Zory, "Distributed feedback coupling coefficient in diode lasers with metalized gratings," *IEEE Photon. Technol. Lett.*, vol. 2, pp. 614-616, 1990.

[Luo92]   H. J. Luo and P. S. Zory, "Mid-infrared metalized distributed feedback lead salt lasers," *Florida High Technology and Industry Council Report*, No. 9G408, University of Florida, Gainesville, Florida, 1992.

[Luo93]   H. J. Luo and P. S. Zory, "Ray optics determination of the DFB coupling coefficient in separate confinement and multiquantum well laser structures," *IEEE J. Quantum Electron.*, vol. QE-29, 1993.

[Mac87]   S. H. Macomber, J. S. Mott, R. J. Noll, G. M. Gallatin, E. J. Gratrix, S. L. O'Dwyer and S. A. Lambert, "Surface emitting distributed feedback semiconductor lasers," *Appl. Phys. Lett.*, vol. 51, pp. 472-474, 1987.

[Mak91]   T. Makino and D. M. Adams, "TE- and TM-coupling coefficients in multiquantum well distributed feedback lasers," *IEEE Photo. Tech. Lett*, vol. 3, pp. 963-965, 1991.

[Mar72]   D. Marcuse, "Higher-order scattering losses in dielectric waveguides," *Bell Sys. Tech. J.*, vol. 51, pp. 1801-1817, 1972.

[Moh86]   M. G. Moharam and T. K. Gaylord, "Rigorous coupled-wave analysis of metallic surface-relief gratings," *J. Opt. Soc. Am.*, vol. A3, pp. 1780-1787, 1986.

[Mot89]   J. S. Mott and S. H. Macomber, "Two-dimensional surface emitting distributed feedback laser arrays," *IEEE Photo. Tech. Lett.*, vol. 1, pp. 202-204, 1989.

[Nol90]   R. J. Noll and S. H. Macomber, "Analysis of grating surface emitting lasers," *IEEE J. Quantum Electron.*, vol. QE-26, pp. 456-466, 1990.

[Pal85]   E. D. Palik, ed., *Handbook of Optical Constants of Solids*, New York: Academic, 1985.

[Pet80]   R. Petit, ed., *Electromagnetic Theory of Gratings*, New York: Springer-Verlag, 1980.

[Ras91]   A. Rast and A. Zach, "Room temperature cw operation of λ=1.55μm InGaAsP/InP ITG-DFB-BCRW lasers with contacted surface grating," *Electron. Lett.*, vol. 27, pp. 108-109, 1991.

[Rig76]   W. W. Rigrod and D. Marcuse, "Radiation loss
          Coefficients of Asymmetric Dielectric Waveguides
          with shallow sinusoidal corrugations," *IEEE J.
          Quantum Electron.*, vol. QE-12, pp. 673-685, 1976.

[Sak82]   K. Sakai, K. Utaka, S. Akiba and Y. Matsushima,
          "1.5μm range InGaAsP/InP distributed feedback
          lasers," *IEEE J. Quantum Electron.*, vol. QE-18, pp.
          1272-1278, 1982.

[Sam90]   R. A. Sammut and I. M. Skinner, "Effective index
          models for MQW waveguides," *Optics Commun.*, vol.
          76, pp. 213-216, 1990.

[Sha88]   Y. Shani, A. Katzir, M. Tacke and H. M. Preier,
          "Metal clad $Pb_{1-x}Sn_xSe/Pb_{1-x-y}Eu_ySn_xSe$ distributed
          feedback lasers," *IEEE J. Quantum Electron.*, vol.
          QE-24, pp. 2135-2137, 1988.

[Sha89]   Y. Shani, A. Katzir, M. Tacke and H. M. Preier,
          "$Pb_{1-x}Sn_xSe/Pb_{1-x-y}Eu_ySn_xSe$ corrugated diode lasers,"
          IEEE J. Quantum Electron., vol. QE-25, pp. 1828-
          1844, 1989.

[Str75]   W. Streifer, D. R. Scifres and R. D. Burnham,
          "Coupling coefficients for distributed feedback
          single- and double-heterostructure diode lasers,"
          IEEE J. Quantum Electron., vol. QE-11, pp. 867-873,
          1975.

[Str77]   W. Streifer, D. R. Scifres, R. D. Burnham and R. I.
          MacDonald, "On grating-coupled radiation from
          waveguides," *IEEE J. Quantum Electron.*, vol. QE-13,
          pp. 67-68, 1977.

[Sug82]   A. Sugimura, "Band-to-band Auger effect in long
          wavelength multinary III-V alloy semiconductor
          lasers," *IEEE J. Quantum Electron.*, vol. QE-18, pp.
          352-363, 1982.

[Tak92]   S. Takigawa, K. Bacher, L. B. Aronson and J. S.
          Harris, "Low threshold current grating-coupled
          surface-emitting strained-InGaAs single quantum
          well laser with GaAs optical confinement
          structure," *Appl. Phys. Lett.*, vol. 60, pp. 265-
          267, 1992.

[Tam90]   T. Tamir, ed., *Guided-Wave Optoelectronics*, New
          York: Springer-Verlag, 1990.

[Tod86]   S. Todoroki, "Influence of local heating on current-optical output power characteristic in $Ga_{1-x}Al_xAs$ lasers," *J. Appl. Phys.*, vol. 60, pp. 61-65, 1986.

[Tsa92]   W. T. Tsang, F. S. Choa, M. C. Wu, Y. K. Chen, R. A. Logan, A. M. Sergent and C. A. Burrus, "Long-wavelength InGaAsP/InP distributed feedback lasers incorporating gain-coupled mechanism," *IEEE Photon. Technol. Lett.*, vol. 4, pp. 212-215, 1992.

[Wal77]   J. N. Walpole, A. R. Calawa, S. R. Chinn, S. H. Groves and T. C. Harman, "CW operation of distributed feedback $Pb_{1-x}Sn_xTe$ lasers," *Appl. Phys. Lett.*, vol. 30, pp. 524-526, 1977.

[Yan81]   M. Yano, H. Imai, K. J. Hori and M. Takusagawa, "High temperature characteristics of stripe-geometry InGaAsP/InP double-heterostructure lasers," *IEEE J. Quantum Electron.*, vol. QE-17, pp. 619-626, 1981.

[Yar73]   A. Yariv, "Coupled-mode theory for guided-wave optics," *IEEE J. Quantum Electron.*, vol. QE-9, pp. 919-933, 1973.

[Zor75]   P. Zory and L. D. Comerford, "Grating-coupled double-heterostructure AlGaAs diode lasers," *IEEE J. Quantum Electron.*, vol. QE-11, pp. 451-457, 1975.

[Zor92]   P. Zory, "Introduction to diode lasers," *OPTCON'92 short course notes SC07*, Boston, Massachusetts, November 1992.

[Zor93]   P. Zory, ed., *Quantum Well Lasers*, New York: Academic, 1993.

BIOGRAPHICAL SKETCH

Horng-Jye Luo was born in Taiwan in 1962. He received the B.S. degree in electrical engineering from National Taiwan University in 1985. He joined the Noise Research Laboratory at the University of Florida in 1987, working on low frequency noise studies of silicon devices. Since 1989 he has been with the Photonics Research Laboratory at UF, involved in the design, fabrication and characterization of semiconductor lasers. Currently he is working toward the Ph.D. degree, about to finish his dissertation on shiny contact and distributed feedback diode lasers. His area of interest includes lasers, optoelectronics and semiconductor devices.

I certify that I have read this study and that in my opinion it conforms to acceptable standards of scholarly presentation and is fully adequate, in scope and quality, as a dissertation for the degree of Doctor of Philosophy.
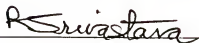
P. Zory, Chairman
Professor of Electrical Engineering

I certify that I have read this study and that in my opinion it conforms to acceptable standards of scholarly presentation and is fully adequate, in scope and quality, as a dissertation for the degree of Doctor of Philosophy.

S. Li
Professor of Electrical Engineering

I certify that I have read this study and that in my opinion it conforms to acceptable standards of scholarly presentation and is fully adequate, in scope and quality, as a dissertation for the degree of Doctor of Philosophy.
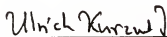
T. Nishida
Assistant Professor of
    Electrical Engineering

I certify that I have read this study and that in my opinion it conforms to acceptable standards of scholarly presentation and is fully adequate, in scope and quality, as a dissertation for the degree of Doctor of Philosophy.

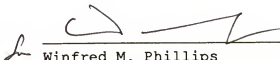R. Srivastava
Professor of Electrical Engineering

I certify that I have read this study and that in my opinion it conforms to acceptable standards of scholarly presentation and is fully adequate, in scope and quality, as a dissertation for the degree of Doctor of Philosophy.

U. Kurzweg
Professor of Aerospace Engineering,
  Mechanics and Engineering Science

This dissertation was submitted to the Graduate Faculty of the College of Engineering and to the Graduate School and was accepted as partial fulfillment of the requirements for the degree of Doctor of Philosophy.

August 1993

Winfred M. Phillips
Dean, College of Engineering

Dean, Graduate School